Published in final edited form as:

Cancer Res. 2019 July 15; 79(14): 3636–3650. doi:10.1158/0008-5472.CAN-18-2931.

Asporin Restricts Mesenchymal Stromal Cell Differentiation, Alters the Tumor Microenvironment, and Drives Metastatic Progression

Robert M. Hughes[1,2,3], **Brian W. Simons**[1], **Hamda Khan**[1,2,3], **Rebecca Miller**[1,2,3], **Valentina Kugler**[1,2,3], **Samantha Torquato**[1,2,3], **Debebe Theodros**[2,3], **Michael C. Haffner**[2,3,4], **Tamara Lotan**[2,3,4], **Jessie Huang**[5], **Elai Davicioni**[6], **Steven S. An**[2,3,5,7], **Ryan C. Riddle**[8], **Daniel L. J. Thorek**[9], **Isla P. Garraway**[10], **Elana J. Fertig**[2,3], **John T. Isaacs**[1,2,3], **W. Nathaniel Brennen**[2,3], **Ben H. Park**[2,3,7], **Paula J. Hurley**[1,2,3,*]

[1]The James Buchanan Brady Urological Institute, Department of Urology, Johns Hopkins School of Medicine, Baltimore, MD, USA

[2]The Department of Oncology, Johns Hopkins School of Medicine, Baltimore, MD, USA

[3]The Sidney Kimmel Cancer Center, Johns Hopkins School of Medicine, Baltimore, MD, USA

[4]The Department of Pathology, Johns Hopkins School of Medicine, Baltimore, MD, USA

[5]The Department of Environmental Health and Engineering, Johns Hopkins Bloomberg School of Public Health, Baltimore, MD, USA

[6]Genome Dx Biosciences, Inc., Vancouver, BC, Canada

[7]The Whiting School of Engineering, Department of Chemical and Biomolecular Engineering, Johns Hopkins University, Baltimore, MD

[8]The Department of Orthopedic Surgery, Johns Hopkins School of Medicine, Baltimore, MD, USA

[9]The Department of Radiology, Johns Hopkins School of Medicine, Baltimore, MD, USA

[10]The Department of Urology, David Geffen School of Medicine at UCLA, Los Angeles, CA, USA

Abstract

Tumor progression to metastasis is not cancer cell autonomous, but rather involves the interplay of multiple cell types within the tumor microenvironment. Here we identify Asporin (ASPN) as a novel, secreted mesenchymal stromal cell (MSC) factor in the tumor microenvironment that regulates metastatic development. MSCs expressed high levels of ASPN, which decreased following lineage differentiation. ASPN loss impaired MSC self-renewal and promoted terminal cell differentiation. Mechanistically, secreted ASPN bound to BMP-4 and restricted BMP-4-induced MSC differentiation prior to lineage commitment. ASPN expression was distinctly

[*]**Correspondence:** Paula J. Hurley. Johns Hopkins University. 1550 Orleans Street CRBII 146. Baltimore, MD 21231. 410-614-9453. phurley2@jhmi.edu.

Disclosure of Potential Conflicts of Interest

Elai Davicioni is the President and CSO, Director of GenomeDx. Ben H. Park is a consultant for Foundation Medicine, Roche, H3 Biomedicine, Casdin Capital, Loxo Oncology, and Lilly, all outside the submitted work. No potential conflicts of interest were disclosed by the other authors.

conserved between MSC and cancer-associated fibroblasts (CAF). ASPN expression in the tumor microenvironment broadly impacted multiple cell types. Prostate tumor allografts in ASPN-null mice had a reduced number of tumor-associated MSCs, fewer cancer stem cells, decreased tumor vasculature, and an increased percentage of infiltrating CD8+ T cells. ASPN-null mice also demonstrated a significant reduction in lung metastases compared to wild type mice. These data establish a role for ASPN as a critical MSC factor that extensively effects the tumor microenvironment and induces metastatic progression.

Keywords

Asporin; Mesenchymal Stem Cell; Mesenchymal Stromal Cell; Activated Fibroblast; Reactive Stroma; Cancer-Associated Fibroblast; Tumor Microenvironment; Prostate Cancer; Bone Morphogenetic Protein-4; Differentiation; Self-renewal; Metastasis

Introduction

Tumors do not develop in isolation and components of the tumor microenvironment demonstrably influence many cancer hallmarks including metastasis (1, 2). A growing body of evidence now indicates that cells of mesenchymal origin including mesenchymal stem cells, mesenchymal stromal cells, and fibroblasts, collectively referred to herein as MSCs, reside in the tumor microenvironment and contribute to cancer progression (2-5). MSCs are a heterogeneous population of multipotent stromal cells that give rise to physiologic cell lineages including osteoblasts, adipocytes, and chondrocytes (6). MSCs also give rise in part to pathological cell lineages including cancer-associated fibroblasts (CAFs) and fibroblasts associated with injury or inflammation (2, 3, 7, 8). Similar to MSCs, CAFs are highly heterogeneous and dynamic, which may account for the reported pleiotropic roles of MSCs and CAFs in cancer progression as either potentiators of primary and metastatic cancer development (4, 5, 9-14) or restrainers of cancer growth (15-17). The seminal properties of MSCs in the tumor microenvironment have yet to be fully established. Due to the conservation between gene expression programs in development and cancer (18, 19), key factors may be similar between MSCs in development and MSCs in the tumor microenvironment.

Asporin (ASPN), a member of the small leucine-rich proteoglycan (SLRP) family of extracellular proteins, is markedly enriched in fetal prostate mesenchyme during development (18, 20). ASPN is similarly expressed in reactive stromal cells, including CAFs, in the tumor microenvironment of prostate (20-22), breast (23), scirrhous gastric (24), and pancreatic (25) cancers. The role of ASPN in prostate MSCs and in the tumor microenvironment is poorly understood. Intriguingly, ASPN has been reported to regulate mediators of MSC differentiation including BMP-2 (26) and TGF-β1 (27). Yet, the roles of ASPN in MSC self-renewal and multipotency have not been definitively determined.

ASPN has been shown to induce migration of scirrhous gastric (24, 28) and pancreatic (25) cancer cells; nevertheless, ASPN expression in the tumor microenvironment may have a dual role in regulating cancer progression (21-25, 29), possibly due to polymorphisms in the ASPN aspartic acid (D)-repeat domain length (21). ASPN expression in prostate reactive

stromal cells is associated with adjacent local cancer aggressiveness and with worse oncologic outcomes (21, 22). However, two, of the over 10 reported, germline polymorphisms in the ASPN D-repeat domain length have been shown to be differentially associated with the development of metastatic prostate cancer following surgery (21). *ASPN* with 14 D-repeats (*ASPN* D14) was associated with an increased risk while *ASPN* D13 was associated with a reduced risk of metastatic progression (21).

Herein, we report that ASPN functions as a novel, secreted MSC factor and a key driver of metastatic development. We establish a role for ASPN in regulating fundamental properties of MSCs including self-renewal, differentiation, and migration. We demonstrate that ASPN expression is highly enriched in MSCs, and its expression decreases during differentiation to connective tissue lineages. Our data show that ASPN regulates MSC self-renewal and restricts MSC differentiation through regulation of BMP-4 signaling. ASPN null mice have fewer MSCs in the bone marrow and an enriched population of intermediate (or more differentiated) MSCs in the prostate. While most MSC-derived progeny have decreased ASPN expression, high ASPN expression is conserved between MSCs and CAFs in both primary and metastatic tumors. Prostate allograft tumors in ASPN null mice have an altered tumor microenvironment with fewer tumor-associated MSCs, decreased vasculature, and an increased percentage of infiltrating CD8+ T cells. Tumors in ASPN null mice also have a reduced number of cancer stem cells and a marked decrease in metastatic potential. These findings suggest that ASPN is an important regulator of MSC multipotency and metastatic development.

Materials and Methods

Immunohistochemistry (30), immunofluorescence (30), immunoblotting (21), RNA isolation and quantitative real-time PCR (30), colony forming unit assay (31), cell proliferation (32), migration (32), cytoskeletal remodeling (32), MSC isolation and differentiation (5, 30, 32-36), the PELICAN study (37), and the CP1 *E. coli* model of prostate inflammation (38) have been previously described and are detailed in the Supplementary Materials and Methods.

Cell lines and cell culture

PC-3, DU-145, WPMY-1, TRAMP-C2, and HEK293T cell lines were obtained from the American Type Culture Collection (ATCC). The B6MycCaP cancer cell line was a kind gift from Dr. Leigh Ellis (Roswell Park Cancer Institute). All cell lines were maintained in either DMEM (DU-145, WPMY-1, TRAMP-C2, B6MycCaP) or RPMI 1640 (PC-3) supplemented with 10% fetal bovine serum (Corning), and penicillin/streptomycin (Life Technologies). Following thaw from frozen stock, cell lines were used prior to passage 7. The WPMY-1-ASPN variant expressing cell lines were generated and cultured as previously described (21). Human MSCs were isolated from tissue and cultured in RoosterNourish™-MSC (RoosterBio) as previously described (5, 39). Mouse MSCs were cultured in DMEM supplemented with 10% fetal bovine serum (Corning), Glutamx (Life Technologies) and penicillin/streptomycin (Life Technologies). B6CaP organoids were generated from C57BL/6J Hi-Myc allografts and cultured using an adapted protocol from prior reports (40,

41). Briefly, B6CaP allograft tumors were finely minced with a scalpel, digested in DMEM/F12 + 10% FBS + 1:10 dilution of collagenase/hyaluronidase for one hour at 37°C, triturated in pre-warmed 1X PBS + DNAse I, and filtered through a 40μm cell strainer. Cells were embedded in growth factor reduced (GFR) Matrigel, plated on ultra-low attachment plates (Corning), and cultured in Advanced DMEM/F12 supplemented with 10% charcoal-stripped FBS, B-27, GlutaMAX, HEPES, and penicillin/streptomycin, recombinant mouse EGF (10ng/mL), TGF-β inhibitor A83-01 (200nM), ROCK inhibitor Y-27632 (10μM), and DHT (100nM). For harvest and passage, Matrigel-embedded organoids were incubated in pre-warmed Dispase (5U/mL) and subsequently trypsinized for single cell isolation. Cell lines were authenticated by STR analysis and confirmed mycoplasma free by PCR testing (JHU Genetic Resources Core Facility).

Prostate cancer and inflammation study

Tissue from radical prostatectomies performed at Johns Hopkins School of Medicine from 2009 to 2011 were examined for ASPN expression in cancer adjacent stroma and in inflammation adjacent stroma. Four-micrometer-cut radical prostatectomy sections were stained for ASPN (Sigma) by IHC. Cases were scored by a urologic pathologist for ASPN expression in stroma adjacent to cancer and in distinct areas of stroma adjacent to chronic inflammation. Chronic inflammation was defined by clusters of 20 or more lymphocytes. Of the 15 cases selected, 13 cases contained both cancer and distinct areas of chronic inflammation. Using established scoring schemes (21), ASPN intensity was evaluated and assigned an incremental score of 0 (negative), 1 (weak), 2 (moderate), or 3 (strong). The extent of staining was assigned a percentage from 0-100%. An ASPN score was calculated by multiplying the intensity score and the extent score (H-score).

Aspn$^{-/-}$ mice

All animal procedures were performed under a JHU approved Institutional Animal Care and Use Committee (IACUC) protocol. Mice were purchased from The Jackson Laboratory and maintained under standard pathogen free conditions. B6;129S5-*Aspn*^{tm1Lex}/Mmucd were generated through the Mutant Mouse Regional Resource Center (MMRRC) at UC Davis, a NIH funded strain repository. B6;129S5-*Aspn*^{tm1Lex} were donated to MMRRC by Genentech, Inc. Exon 2 was targeted (NCBI accession AF316825.1) by homologous recombination. The embryonic stem cell (ESC) line was derived from 129S5/SvEvBrd from Lexicon Genetics. B6;129S5-*Aspn*^{tm1Lex} mice were then fully backcrossed at least 9 generations to the C57BL/6J background. Mice were genotyped by PCR of genomic DNA with wild-type and mutation specific primers.

B6CaP model of metastasis

The B6CaP allograft model was derived from a C57BL/6J Hi-Myc mouse metastatic lesion. Cells from the metastatic tissue were isolated and serially passaged in C57BL/6J mice. When injected subcutaneously with B6CaP allograft cells, 60-70% of C57BL/6J mice develop lung metastases. For this study, we injected 5.5×10^6 B6CaP cells in 100μL PBS subcutaneously into *Aspn*$^{+/+}$, *Aspn*$^{+/-}$, and *Aspn*$^{-/-}$ mice (n=6 mice per group), resected tumors once they reached $1cm^3$, waited 11 weeks post-resection, euthanized the mice and

inspected the lungs for metastases. Lungs were formalin-fixed, paraffin-embedded, sectioned, and stained as described previously (42).

Flow cytometry

To assess the *in vivo* MSC population in adult mouse prostates or B6CaP tumors by flow cytometry, the tissue of interest was isolated, mechanically dissociated, digested in RPMI + 10% FBS + 1:10 dilution of collagenase/hyaluronidase for one hour at 37°C, triturated in prewarmed PBS + DNAse I, and filtered through a 40μm cell strainer. If necessary, red blood cells were lysed by briefly incubating the cell pellet in ice-cold ACK lysis buffer (Quality Biological). Cells were Fc-blocked (Miltenyi) for 10 minutes in 4°C. Dead cells were discriminated using the LIVE/DEAD Fixable Aqua Dead Cell Stain Kit (Thermo Fisher Scientific) and samples were stained with the following antibodies from BioLegend: CD45, CD29, CD105, Sca-1, Ly6G, Ly6C, CD11b, CD11c, CCR2, F4/80, MHC II, CD3, CD4, CD8a, FoxP3, CD44, CD62L as well as CD3 from BD Pharmingen. Stained samples were analyzed on an LSR II flow cytometer (BD) and quantified using FlowJo.

Co-immunoprecipitation assays

HEK293T cells were transfected with a murine ASPN-Myc-FLAG tagged expression vector (Origene) or vehicle control using Lipofectamine 3000 (Thermo Fisher Scientific) according to the manufacturer's protocol. Two days post-transfection, cells were washed with PBS and incubated in serum-free DMEM overnight. HEK293T cells were then treated with 0.3μg/mL recombinant murine BMP-4 protein (R&D Systems) or vehicle and incubated in 5% CO2 at 37°C for 30 minutes. Following BMP-4 incubation, conditioned media was filtered through a 0.45μm filtration unit (Millipore) and one third was set aside for the "input" sample. The remaining two thirds was treated with a protease inhibitor cocktail (Sigma), pre-cleared with mouse IgG agarose (Sigma) for one hour rotating at 4°C, and then incubated with anti-FLAG M2 magnetic beads (Sigma) overnight rotating at 4°C. Beads were washed three times with ice cold TBS, and proteins were eluted from the beads with 3XFLAG peptide (Sigma). Input conditioned media was concentrated using an Amicon Ultra-4 centrifugal filter unit with a 10kDa NMWL (Millipore) according to the manufacturer's protocol.

Gene expression analysis

Gene expression profiling was performed for *Aspn*$^{+/+}$ and *Aspn*$^{-/-}$ fetal MSCs expanded to passage 3 and cultured under normal growth conditions to 70-80% confluency prior to RNA isolation. Three biological replicates were analyzed per experimental group and Affymetrix mouse Clariom D arrays were run. Bioinformatics analyses were performed in R. Datasets were normalized at a transcript level for core transcripts with the R/Bioconductor package oligo and annotated with the NetAffx Biological Annotations. Artifacts from technical batches were removed with ComBat (43) implemented in the R/Bioconductor package SVA (44). Differential expression analyses were performed on ComBat adjusted data using the R/Bioconductor package LIMMA (45). Genes with FDR adjusted p-values below 0.05 and absolute log fold change greater than or equal to two were called statistically significant. Gene set analysis was performed on the KEGG cell cycle pathway and the GeneMAPP TGF-β family signaling pathway obtained from the NetAffx Biological Annotations to

confirm hypothesized functional mechanisms with a one-sided Wilcoxon gene set test implemented in LIMMA.

Quantification and statistical analysis

Unless otherwise indicated, statistical comparisons between two groups were performed using a two-tailed unpaired Student's t-test. Statistical comparisons between multiple groups were performed using one-way Analysis of Variance (ANOVA) with Tukey or Newman-Keuls multiple comparisons, as indicated in the figure legends. Statistical significance was defined as a P value <0.05, and P values were indicated with asterisks in the figures as follows: *P≤0.05; **P≤0.01; ***P≤0.001; ****P≤0.0001. All statistical comparisons were performed using GraphPad Prism software (v5.0).

Results

ASPN is Highly Expressed in MSCs

ASPN expression was examined in primary human MSCs isolated from fetal prostate, benign prostate, prostate cancer, and bone marrow. Primary heterogeneous cultures were expanded and shown to be enriched for MSCs by flow cytometry expression profile ($CD73^+$, $CD90^+$, $CD105^+$, $CD14^-$, $CD20^-$, $CD34^-$, $CD45^-$, and $HLA\text{-}DR^-$) and by multi-lineage (osteoblast, adipocyte, and chondrocyte) differentiation potential (5). Compared to human primary benign prostate epithelial cells (PreC) and a human benign prostate epithelial cell line (RWPE-1), MSCs from all sites had significantly elevated *ASPN* expression (Fig. 1A). Similar to human MSCs (20), *Aspn* mRNA and protein were distinctly expressed in urogenital sinus mesenchyme (UGM) compared to urogenital sinus epithelium (UGE) of the developing mouse prostate (Fig. 1B, C). MSCs were isolated from both fetal and adult mouse prostate and adult mouse bone-marrow, expanded in culture, and then examined for *Aspn* expression. Mouse MSCs showed increased *Aspn* expression compared to UGE (Fig. 1B). In contrast to MSCs and fetal prostate mesenchyme, ASPN expression was markedly reduced in adult mouse benign prostate stromal cells as determined by IHC (Fig. 1C). These data suggest that ASPN is highly expressed in both bone-marrow derived and tissue resident human and mouse MSCs. However, the role of ASPN in regulating key properties of MSCs such as self-renewal, differentiation, and migration has not been fully established.

ASPN Regulates MSC Self-renewal

To determine the role of ASPN in MSCs, we generated $Aspn^{-/-}$ mice (B6J-$Aspn^{tm1Lex}$/Mmucd), which were then fully backcrossed at least 9 generations to the C57BL/6J background. The first coding exon of *Aspn*, exon 2, was targeted for deletion by homologous recombination (46) (Supplementary Fig. S1A, B), which resulted in the loss of full-length *Aspn* transcript and protein (Supplementary Fig. 1C, D). $Aspn^{-/-}$ mice were viable, fertile, had comparable prostate size and histology, and had similar expression of other SLRP family members including *Decorin* (*Dcn*), *Biglycan* (*Bgn*), and *Extracellular matrix protein 2* (*Ecm2*) as $Aspn^{+/+}$ mice (Supplementary Fig. S1E-K).

To determine how ASPN regulates MSCs *in vivo*, we compared bone marrow-derived MSCs from $Aspn^{+/+}$ and $Aspn^{-/-}$ male mice at 24 weeks of age by flow cytometry for MSC

markers ($CD45^{-}$, $CD105^{+}$, $CD29^{+}$, and $Sca\text{-}1^{+}$). By these markers, both *Aspn*$^{+/+}$ and *Aspn*$^{-/-}$ mice had a single population of bone marrow-derived MSCs; however, *Aspn*$^{-/-}$ bone marrow had significantly fewer MSCs than bone marrow from *Aspn*$^{+/+}$ mice (Fig. 1D and Supplementary Fig. S2A, B). We next compared prostate MSCs from *Aspn*$^{+/+}$ and *Aspn*$^{-/-}$ male mice at 24 weeks of age. In contrast to the single MSC population detected in the bone marrow, both *Aspn*$^{+/+}$ and *Aspn*$^{-/-}$ prostates had two distinct populations of MSCs which were delineated by the level of Sca-1 expression ($Sca\text{-}1^{hi}$ vs. $Sca\text{-}1^{med}$) (Supplementary Fig. S2C, D). Prior studies have shown that MSC stem progenitors with the capacity for both self-renewal and differentiation are $Sca\text{-}1^{hi}$, while more differentiated intermediate MSC progenitors with proliferative and differentiation capacity but with reduced self-renewal ability are $Sca\text{-}1^{med}$ (47). Interestingly, *Aspn*$^{-/-}$ prostates were slightly enriched for $Sca\text{-}1^{med}$ intermediate MSCs compared to *Aspn*$^{+/+}$ prostates (Fig. 1E, Supplementary Fig. S2C, D) suggesting that in the absence of ASPN, prostate-derived MSCs are more likely to differentiate and may thereby have a decreased potential for self-renewal.

To examine MSC self-renewal *in vitro*, total MSCs were isolated from *Aspn*$^{+/+}$ and *Aspn*$^{-/-}$ bone marrow, compact bone, and prostates at 24 weeks of age and then plated at equal numbers *in vitro* for colony forming unit (CFU) assays. Compared to *Aspn*$^{+/+}$, *Aspn*$^{-/-}$ bone marrow-, compact bone-, and prostate-derived MSCs formed significantly fewer CFUs (Fig. 1F-K and Supplementary Fig. S3A, B). To determine further the role of ASPN in self-renewal, fetal MSCs were isolated from *Aspn*$^{+/+}$ and *Aspn*$^{-/-}$ mice and examined at early (P2) and late (P7) passage for CFU ability. CFU number was comparable between early passage *Aspn*$^{-/-}$ and *Aspn*$^{+/+}$ fetal MSCs; however, late passage *Aspn*$^{-/-}$ fetal MSCs formed significantly fewer colonies compared to late passage *Aspn*$^{+/+}$ fetal MSCs (Fig. 1L-N and Supplementary Fig. S3C, D). When added to late passage *Aspn*$^{-/-}$ fetal MSCs, recombinant mouse ASPN did not increase CFU number. Collectively, these data suggest that ASPN is necessary to sustain a sub-population of MSCs with self-renewal capacity, but exogenous ASPN is not able to rescue self-renewal once MSCs have lost this capacity.

ASPN Restricts MSC Proliferation and Differentiation

The loss of bone marrow MSCs in *Aspn*$^{-/-}$ mice suggests that ASPN may regulate MSC differentiation. Consistent with a more quiescent phenotype, *Aspn*$^{+/+}$ fetal MSCs had a significantly decreased proliferation rate compared to *Aspn*$^{-/-}$ fetal MSCs (Fig. 2A). Microarray analyses of gene expression changes between *Aspn*$^{+/+}$ and *Aspn*$^{-/-}$ fetal MSCs demonstrated that genes annotated to the cell cycle by KEGG were significantly downregulated in *Aspn*$^{+/+}$ compared to *Aspn*$^{-/-}$ fetal MSCs (Fig. 2B). Consistent with a more proliferative phenotype, *Aspn*$^{-/-}$ fetal MSCs had elevated expression of several DNA synthesis regulatory genes including *Cdc45*, *Mcm2, Mcm3, Mcm5*, and *Mcm6*. In contrast, *Aspn*$^{+/+}$ fetal MSCs showed increased expression of genes that restrict cell cycle progression including *Cdkn2a*. Interestingly, two genes with reported germline SNPs associated with aggressive prostate cancer, *Cdkn1a* and *Cdkn1b* (48), were differentially elevated between *Aspn*$^{+/+}$ and *Aspn*$^{-/-}$ MSCs.

To more clearly define the role of ASPN in regulating MSC differentiation, early passage (P3) fetal MSCs from *Aspn*$^{+/+}$ and *Aspn*$^{-/-}$ mice were cultured in osteogenic, adipogenic,

and chondrogenic differentiation-inducing media and then analyzed for *in vitro* lineage differentiation. Differentiation to all three lineages (osteoblast, adipocyte, and chondrocyte) was significantly greater in *Aspn*$^{-/-}$ fetal MSCs compared to *Aspn*$^{+/+}$ fetal MSCs as measured by Alizarin Red, Oil Red O, and Alcian Blue staining, respectively (Fig. 2C-H). In addition, lineage-specific differentiation markers such as *Runx2*, *Adipoq*, and *Col10a1* were significantly higher in *Aspn*$^{-/-}$ fetal MSCs compared to *Aspn*$^{+/+}$ fetal MSCs when cultured in osteogenic, adipogenic, and chondrogenic differentiation-inducing media, respectively (Fig. 2I-K). Compared to control media, *Aspn* expression in *Aspn*$^{+/+}$ fetal MSCs significantly decreased in differentiation-inducing media, indicating that *Aspn* is downregulated during differentiation (Fig. 2L-N). Consistent with these findings, recombinant mouse ASPN decreased osteogenic differentiation of *Aspn*$^{-/-}$ fetal MSCs (Supplementary Fig. S3E, F). Interestingly, late passage (P8) *Aspn*$^{-/-}$ fetal MSCs showed increased differentiation in the absence of differentiation-inducing media (Supplementary Fig. S3G-K). Collectively, these data suggest that ASPN restricts MSC proliferation and inhibits early MSC differentiation prior to lineage specification.

ASPN Binds to BMP-4 and Restricts BMP-4-induced Signaling and Differentiation

How ASPN regulates MSC differentiation is not fully known. ASPN has been reported to regulate many extracellular signaling molecules (27, 28, 49-52), including multiple TGF-β family members (26, 27, 49, 51-53). Most TGF-β family members have pleiotropic and lineage-specific roles during differentiation; however, BMP-4 distinctly induces progenitor differentiation to osteoblast, adipocyte, and chondrocyte lineages (54). Microarray analysis of gene expression changes between *Aspn*$^{+/+}$ and *Aspn*$^{-/-}$ fetal mouse MSCs demonstrated that TGF-β family signaling pathway genes annotated in GeneMAPP, including genes restricted to BMP signaling, were significantly downregulated in *Aspn*$^{+/+}$ compared to *Aspn*$^{-/-}$ fetal MSCs (Fig. 3A). Consistent with this, BMP-4-induced SMAD1/5/9 phosphorylation was significantly decreased in *Aspn*$^{+/+}$ compared to *Aspn*$^{-/-}$ fetal mouse MSCs (Fig. 3B, C). Similarly, recombinant mouse ASPN also restricted BMP-4-induced signaling in *Aspn*$^{-/-}$ fetal mouse MSCs (Fig. 3D, E).

Prior studies have shown that polymorphisms in the aspartic acid (D)-repeat length of human ASPN differentially regulate signaling (27) and that germline D-repeat variants are differentially associated with prostate oncologic outcomes (21). The germline variant of human ASPN containing 14-D repeats (ASPN D14) was shown to be significantly associated with metastatic prostate cancer recurrence after surgery while homozygosity for the ASPN D13 variant was significantly associated with a reduced risk of metastatic recurrence (21). To determine if ASPN D14 and ASPN D13 differentially regulate BMP-4 signaling in human prostate stromal cells, we generated independent clones (A and B) of the prostate fibroblast cell line, WPMY-1, overexpressing either ASPN D13 or ASPN D14. Independent clones of WPMY-1 expressing the neomycin empty vector alone (Neo) were also generated as control lines. WPMY-1, which are germline ASPN D13/13, did not express ASPN under standard conditions (Fig. 3F) (21). Similar to mouse ASPN, ASPN D14 significantly restricted BMP-4-induced signaling in WPMY-1 cells compared to WPMY-1-Neo and WPMY-1-ASPN D13 (Fig. 3F, G). BMP-4-induced signaling was

slightly decreased in WPMY-1-ASPN D13 compared to WPMY-1-Neo, but was not significant (Fig. 3F, G).

To determine if ASPN directly binds to BMP-4, mouse ASPN was overexpressed in HEK293T cells and then incubated with recombinant mouse BMP-4. Immunoprecipitation of secreted ASPN from the media demonstrated binding to BMP-4 (Fig. 3H). To determine if BMP-induced signaling is necessary for differentiation in the absence of ASPN, we interrogated the ability of a BMP inhibitor to rescue differentiation in *Aspn*$^{-/-}$ MSCs. To do this, we compared osteogenic-induced differentiation in *Aspn*$^{+/+}$ and *Aspn*$^{-/-}$ fetal MSCs in the absence of BMP-induced signaling by treating MSCs with the BMP inhibitor LDN-193189 or vehicle. Inhibition of BMP-induced signaling significantly restricted osteogenic-induced differentiation in *Aspn*$^{-/-}$ fetal MSCs as assayed by Alizarin Red staining and by expression of osteogenic-induced genes (Fig. 3I, J). To determine if BMP-4 could rescue differentiation in *Aspn*$^{+/+}$ fetal MSCs, we compared osteogenic-induced differentiation in *Aspn*$^{+/+}$ and *Aspn*$^{-/-}$ fetal MSCs in the presence of exogenous recombinant mouse BMP-4. BMP-4 strongly induced differentiation in *Aspn*$^{+/+}$ fetal MSCs (Fig. 3I, J). Taken together, these findings support a model by which mouse ASPN and human ASPN D14 restrict BMP-4-induced signaling and differentiation of MSCs.

ASPN Expression Pattern is Distinctly Conserved between MSCs and Reactive Stromal Cells in the Tumor Microenvironment

MSCs also give rise, in part, to pathological cell lineages including CAFs and injury or inflammation-associated fibroblasts (2, 3, 7, 8, 39, 47, 55, 56). We and others have previously reported that ASPN is highly expressed by reactive stromal cells in the microenvironment of primary tumors, with minimal to undetectable expression by primary adenocarcinoma cells or adenocarcinoma derived cell lines (21-25) (Fig. 4A, B, Supplementary Fig. S4A). In fact, ASPN expression in cancer cell lines negatively correlated with the epithelial marker *EPCAM* (Pearson r: −0.2478; $P<0.0001$) and positively correlated with MSC markers including *THY1* (Pearson r: 0.4064; $P<0.0001$), *ENG* (Pearson r: 0.3607; $P<0.0001$), *VCAM* (Pearson r: 0.1237; $P<0.0001$), and *ALCAM* (Pearson r: 0.0952; $P<0.0019$) (Supplementary Fig. S4A-G) (57). Elevated *ASPN* in primary prostate cancer from the TCGA was significantly associated with a worse disease/progression-free survival (Fig. 4C) (58, 59). Similar to human prostate cancer, both *Aspn* mRNA and protein expression were elevated in the tumor microenvironment of mouse models of prostate adenocarcinoma compared to benign adjacent prostate stroma and stroma associated with mouse prostatic intraepithelial neoplasia (mPIN) (Fig. 4D-G and Supplementary Fig. S4H).

To determine if ASPN is also expressed in the metastatic tumor microenvironment, prostate cancer metastases from a Johns Hopkins School of Medicine rapid autopsy cohort (n=15 patients; 60 metastases) (37) were analyzed for ASPN expression by immunohistochemistry (IHC) and quantified by H-score. Elevated ASPN expression was detected in reactive stromal cells at various metastatic sites including lymph node, bone, and soft tissue such as lung and liver (Fig. 4H and Supplementary Fig. S4I). ASPN expression in metastatic prostate cancer adjacent stroma was elevated compared to benign prostate, lymph node,

lung, and liver stroma, and it was comparable to ASPN expression in primary prostate cancer (Gleason Sum ≥6) adjacent stroma (Fig. 4I). Thus, we demonstrate that ASPN is highly expressed in MSCs isolated from multiple sites and in reactive stromal cells associated with both primary and metastatic prostate cancers.

To determine if ASPN expression is selective to reactive stroma in the tumor microenvironment or is generally conserved among reactive stroma, we next examined ASPN expression in human and mouse reactive stroma associated with prostate inflammation. Human prostate sections obtained after radical prostatectomy for prostate cancer that contained regions of both benign chronic inflammation and prostate cancer, but in distinct locations (≥2mm apart), were analyzed for ASPN expression by IHC. Compared to reactive stroma associated with human prostate cancer, stroma associated with distinct areas of chronic prostate inflammation expressed significantly lower levels of ASPN that were comparable to benign adjacent stroma (Fig. 4J, K). Similar to human prostate inflammation, CP1 *E. coli*-induced prostate inflammation, which is characterized by a marked vimentin-positive stromal response (38), was largely negative for ASPN expression (Fig. 4L-N). ASPN expression in inflammation adjacent stroma was comparable to benign prostate stroma and was only detected in perivascular regions. Collectively, these data suggest that ASPN expression is selectively conserved between MSCs and cancer-associated reactive stromal cells.

ASPN Induces MSC and Cancer Cell Migration

A fundamental property of MSCs is their ability to migrate to both local and distant areas of tissue injury or damage. Migration was significantly elevated in $Aspn^{+/+}$ mouse fetal MSCs compared to $Aspn^{-/-}$ mouse fetal MSCs (Fig. 5A, B). Consistent with elevated motility, $Aspn^{+/+}$ fetal MSCs cells had increased cytoskeletal remodeling compared to $Aspn^{-/-}$ MSCs as assayed by spontaneous motions of Arg-Gly-Asp (RGD) coated microbeads that bind to the cytoskeletal network through cell surface integrin receptors (Fig. 5C, D). Similar dynamics of increased migration and cytoskeletal remodeling were also observed in WPMY-1-ASPN D14 overexpressing cells compared to WPMY-1-ASPN D13 overexpressing cells and WPMY-1-Neo control cells (Fig. 5E-H).

As a secreted protein in the tumor microenvironment, ASPN may also induce cancer cell migration. We examined cancer cell migration in response to conditioned media from $Aspn^{+/+}$ and $Aspn^{-/-}$ fetal MSCs. Conditioned media from $Aspn^{+/+}$ fetal MSCs increased B6MycCaP (60) and TRAMP-C2 mouse prostate cancer cell migration compared to $Aspn^{-/-}$ fetal MSC conditioned media (Fig. 5I, J and Supplementary Fig. S5A, B). Conditioned media from WPMY-1-ASPN D14 cells also increased PC-3 and DU-145 migration compared to conditioned media from WPMY-1-ASPN D13 cells and conditioned media from WPMY-1- Neo cells (Fig. 5K, L and Supplementary Fig. S5C, D). Interestingly, a 1:1 mix of conditioned media from WPMY-1-ASPN D14 and WPMY-1-ASPN D13 cells also increased PC-3 migration similar to conditioned media from WPMY-1-ASPN D14 alone, thereby suggesting a dominant function of ASPN D14 relative to ASPN D13 (Fig. 5K, L).

ASPN-Induced Migration is Calcium-Dependent

How ASPN regulates prostate stromal and cancer cell migration is not fully understood. Migration in *Aspn*$^{-/-}$ fetal MSCs was neither rescued by the BMP inhibitor LDN-193189 nor further restricted by BMP-4, suggesting that ASPN regulates migration by an alternative mechanism (Supplementary Fig. S5E). To determine if ASPN is able to directly enhance migration as opposed to functioning indirectly through the expression of other secreted factors, migration was examined in *Aspn*$^{-/-}$ cells in the presence of exogenous recombinant mouse ASPN. Elevated migration was observed in *Aspn*$^{-/-}$ cells when cultured with exogenous ASPN (Fig. 6A), suggesting that ASPN can, at least in part, directly enhance migration. To better determine how ASPN regulates migration, *Aspn*$^{+/+}$ MSCs, *Aspn*$^{-/-}$ MSCs, WPMY-1-ASPN D14, WPMY-1-ASPN D13, and WPMY-1-ASPN Neo were compared by microarray for gene expression. Differentially expressed genes in *Aspn*$^{+/+}$ MSCs compared to *Aspn*$^{-/-}$ MSCs as well as in WPMY-1-ASPN D14 compared to WPMY-1-ASPN Neo and in WPMY-1-ASPN D13 compared to WPMY-1-ASPN Neo were examined for KEGG Pathway enrichment. Genes annotated to cell adhesion, actin cytoskeleton, and cytokine-cytokine receptor interaction by KEGG were altered in cells expressing ASPN (*Aspn*$^{+/+}$ MSCs, WPMY-1-ASPN D14, WPMY-1-ASPN D13) compared to cells deficient for ASPN (*Aspn*$^{-/-}$ MSCs and WPMY-1-ASPN Neo) (Supplementary Fig. S5F). Since mouse ASPN and human ASPN D14 enhanced migration compared to ASPN null and ASPN D13 cells, KEGG pathways selective to *Aspn*$^{+/+}$ MSCs and WPMY-1-ASPN D14 were highlighted as a means to determine pathways potentially involved in ASPN-mediated migration. Interestingly, genes annotated to calcium signaling, Hedgehog signaling, chemokine signaling, WNT signaling, and TGFβ signaling by KEGG were altered in *Aspn*$^{+/+}$ MSCs and WPMY-1-ASPN D14 when compared to cells deficient for ASPN (Fig. 6B, C). ASPN has been reported to bind calcium, likely through its poly-aspartate domain (61). Consistent with this, hierarchical clustering showed differential expression of several Gene Ontology (GO) calcium-related genes between *Aspn*$^{+/+}$ and *Aspn*$^{-/-}$ fetal MSCs (Fig. 6D). Similarly, differential expression of calcium-related genes was also observed in WPMY-1-ASPN D14 compared to WPMY-1-ASPN D13 and WPMY-1-Neo (Fig. 6E). To determine if ASPN-mediated migration depends on calcium, *Aspn*$^{-/-}$ MSCs were examined for migration in the presence of exogenous recombinant mouse ASPN and an extracellular calcium chelator, BAPTA. BAPTA restricted ASPN-induced migration suggesting that extracellular calcium is necessary for ASPN's pro-migratory function (Fig. 6F, G).

ASPN Alters the Primary Tumor Microenvironment

To determine the role of ASPN in the tumor microenvironment, we utilized a novel allograft generated from a C57BL/6J Hi-Myc mouse metastatic lesion (B6CaP). This allograft is not to be confused with the B6MycCaP cell line used for migration studies which was generated on a C57BL/6N background (60). B6CaP allografts consisted of both cancer and tumor infiltrating host cells including reactive stromal cells. Due to this stromal infiltration, B6CaP allografts highly expressed *Aspn* (Supplementary Fig. S6A). B6CaP organoids, which were enriched for cancer cells, had undetectable *Aspn* expression further establishing that *Aspn* expression was restricted to infiltrating stromal cells (Supplementary Fig. S6A). Subcutaneous growth of B6CaP allografts was similar in *Aspn*$^{+/+}$, *Aspn*$^{+/-}$, and *Aspn*$^{-/-}$

mice as average tumor volume at resection and average time to resection were not significantly different between mice (Fig. 7A, B). Despite comparable *Aspn* expression at tumor inoculation, B6CaP allografts in $Aspn^{-/-}$ mice had significantly reduced levels of *Aspn* at resection (Supplementary Fig. S6B).

B6CaP allografts were examined for MSCs and CAF-mediated properties including cancer stem cells, immune infiltration, and vascular development. Consistent with our *in vivo* and *in vitro* findings pertaining to the roles of ASPN in MSC self-renewal, differentiation, and migration, flow cytometry demonstrated that B6CaP tumors in $Aspn^{-/-}$ mice had significantly fewer MSCs ($CD45^-$, $CD105^+$, $CD29^+$, and $Sca\text{-}1^+$) compared to B6CaP tumors in $Aspn^{+/+}$ mice (Fig. 7C). B6CaP tumors in $Aspn^{-/-}$ mice also had significantly fewer $CD44^+$ cancer stem cells ($CD45^-$, $CD105^-$, $CD31^-$, $CD29^+$, $Sca\text{-}1^+$, $CD44^+$) compared to B6CaP tumors in $Aspn^{+/+}$ mice (Fig. 7D). Flow cytometry for myeloid and lymphoid lineage cells demonstrated that $Aspn^{-/-}$ tumors had an increased percentage of tumor infiltrating $CD8^+$ T cells compared to $Aspn^{+/+}$ cells (Fig. 7E and Supplementary Fig. S6C, D). IHC for tumor associated vasculature showed that $Aspn^{+/+}$ tumors were enriched for larger blood vessels compared to $Aspn^{-/-}$ tumors (Fig. 7F, G). These findings suggest that ASPN pleiotropically alters both the tumor and the tumor microenvironment.

ASPN Promotes Metastatic Progression

MSCs, cancer stem cells, angiogenesis, and immune infiltration have all been shown to regulate metastatic development. Prior overexpression studies indicate that ASPN (62) and specifically ASPN D14 (21) promotes invasion and metastasis; however, this has not been determined in a genetic, immune-competent mouse model. Thus, we examined metastatic progression in $Aspn^{+/+}$ and $Aspn^{-/-}$ mice with B6CaP allografts. When grown subcutaneously and then resected, B6CaP allografts form lung metastases in 60-70% of C57BL/6J mice. While primary tumor size was similar between $Aspn^{+/+}$ and $Aspn^{-/-}$ mice, the development of lung metastases was strikingly different. B6CaP subcutaneous allografts formed lung metastases in 67% (4/6) of $Aspn^{+/+}$ mice and in 50% (3/6) of $Aspn^{+/-}$ mice, but not in any of the $Aspn^{-/-}$ (0/6) mice (Fig. 7H-J). Collectively, these findings indicate that ASPN in the tumor microenvironment broadly impacts multiple cell types, and ultimately influences metastatic progression (Fig. 7K).

Discussion

MSCs and CAFs reside in the tumor microenvironment and impact cancer growth and progression (4, 5, 9-13). These studies establish ASPN as a novel MSC factor expressed in the tumor microenvironment that regulates metastatic development. ASPN restricts early MSC differentiation, shown here by inhibiting BMP-4 signaling. While ASPN expression is reduced during differentiation to most MSC lineages, ASPN is highly expressed in CAFs and broadly impacts multiple cell types in the tumor microenvironment. Collectively, these findings underpin the role of ASPN as a key mediator of MSC multipotency and as a critical regulator of metastasis in the tumor microenvironment.

MSCs are a heterogeneous population of cells that include cells of mesenchymal origin including mesenchymal stem cells, mesenchymal stromal cells, and fibroblasts. We

demonstrate that ASPN is expressed in MSCs isolated from distinct sites including bone-marrow, adult prostate, and fetal prostate in humans and mice. MSCs give rise to physiologic connective tissue lineages, and differentiation is regulated by both conserved and lineage-specific factors (6). ASPN expression is diminished during MSC differentiation to multiple lineages, and our findings indicate that ASPN functions prior to MSC lineage commitment to suppress the differentiation of a stem population of multipotent MSCs capable of self-renewal. In the absence of ASPN, fewer MSCs reside in the bone marrow and an intermediate population of multipotent MSCs with diminished self-renewal potential predominates in the prostate. This is evidenced by our flow cytometry data demonstrating that in contrast to *Aspn*$^{+/+}$ MSCs in the prostate, MSCs from *Aspn*$^{-/-}$ prostates were enriched for intermediate MSCs (Sca-1^{med}) as opposed to stem MSCs (Sca-1^{hi}). Consistent with these *in vivo* findings, *Aspn*$^{-/-}$ bone marrow-derived, compact bone-derived, prostate-derived, and late passage fetal MSCs had a decreased capacity for self-renewal *in vitro* compared to *Aspn*$^{+/+}$ MSCs. Studies using ASPN deficient cells demonstrated that ASPN restricts MSC differentiation *in vitro* along multiple lineages. Taken together, these data indicate that ASPN functions as a novel MSC factor that maintains MSC multipotency.

MSC lineage commitment and progression through differentiation is regulated by many TGF-β family members (54). ASPN is a secreted extracellular protein that has been shown to antagonize several members of the TGF-β family including BMP-2 (49), BMP-4 (51), and TGF-β1 (27). Most TGF-β family members have pleiotropic roles in regulating MSC differentiation to connective tissue lineages (54). In contrast to other TGF-β family members, BMP-4 distinctly induces early MSC differentiation along several lineages including osteoblasts, adipocytes, and chondrocytes (54). Our data demonstrate that ASPN binds to BMP-4 and restricts BMP-4-induced signaling in MSCs and support a model by which MSC-secreted ASPN locally restricts BMP-4-induced MSC differentiation.

Similar to MSCs, reactive stroma cells in multiple cancer types, including prostate (20-22), breast (23), scirrhous gastric (24), and pancreatic (25), also highly expresses ASPN while benign-associated stroma is largely negative for ASPN expression. In addition to localized cancer, we show that ASPN is widely expressed in prostate cancer metastases. In contrast to the tumor microenvironment, ASPN was not expressed in reactive stroma in the inflammatory microenvironment. This suggests that ASPN expression is not conserved across all types of reactive stroma, but has some specificity to reactive stroma in the tumor microenvironment. Tumor-associated reactive stroma is a heterogeneous population of cells that includes MSCs and CAFs. Studies support that CAFs are in part derived from MSC precursors (47, 55, 56). Accordingly, CAFs may be more similar to MSCs than inflammation-associated reactive stromal cells based on the data presented herein. Collectively, these findings indicate that ASPN expression is highly conserved between MSCs and the reactive stroma in both primary and metastatic tumor microenvironments.

These studies indicate that ASPN broadly impacts both the tumor and the tumor microenvironment. In the absence of ASPN, B6CaP allografts had fewer tumor-associated MSCs supporting that ASPN regulates the number of multipotent MSCs in the tumor microenvironment. In addition, the immune infiltration and vasculature was significantly altered in *Aspn*$^{-/-}$ mice. Effects on other cell types in the tumor microenvironment and on

cancer stem cells may be directly mediated by ASPN or indirectly regulated through MSC deficiencies. In addition to impacting the tumor microenvironment, ASPN may promote tumor progression by directly enhancing migration of both stromal and cancer cells. ASPN has been implicated in the activation of multiple migratory pathways including FGF-2 (50), IGFR (51), RAC1 (24), CD44 (24, 25), and EGFR (28, 62). Our data support that exogenous ASPN is able to enhance migration, likely, by a mechanism independent of its ability to restrict BMP4-induced signaling. Our findings support that ASPN mediated migration is dependent on extracellular calcium and that genes annotated to the KEGG calcium signaling pathway are differentially expressed in ASPN expressing cells compared to ASPN null and ASPN D13 cells. Future studies will be needed to determine how ASPN mechanistically regulates MSC and prostate cancer cell migration.

Mouse and human ASPN are highly homologous, including the D-repeat domain. While C57BL/6 mice have 8 D-repeats interrupted by a single asparagine (N), the D-repeat length in humans is variable. Recent reports suggest that the D-repeat domain length may regulate cancer progression (21, 29). Patients harboring germline allele(s) of *ASPN* D14 were more likely to develop metastatic prostate cancer, while homozygous germline ASPN D13 was associated with a reduced risk of metastatic prostate cancer (21). Animal models have shown that ASPN D14 promotes metastatic prostate cancer progression (21), while ASPN D13 restricts breast (63) and prostate (21) cancer progression. Our data show that ASPN D14 increased stromal and cancer cell migration compared to ASPN D13. Intriguingly, prostate cancer patient-based data suggest that ASPN D14 may be dominant over ASPN D13. Consistent with this, mixed conditioned media from ASPN D13 and ASPN D14 expressing cells increased cancer cell migration similar to conditioned media from ASPN D14 expressing cells alone while conditioned media from ASPN D13 did not increase cancer cell migration. Collectively, our findings reveal that ASPN D14 and ASPN D13 may differentially regulate molecular and cellular pathways that are fundamental to metastasis.

In conclusion, our data identifies ASPN as a novel MSC factor that is conserved in the tumor microenvironment and promotes metastatic progression. Further studies are warranted to determine the efficacy and feasibility of therapeutically targeting ASPN in prostate cancer, and potentially other solid tumor types.

Supplementary Material

Refer to Web version on PubMed Central for supplementary material.

Acknowledgments

We thank Edward M. Schaeffer, Ashley E. Ross, Daniel Ardeljan, Leigh Ellis, Daniele M. Gilkes, Inês Godet, Timothy E. Krueger, and Karen Cravero for thoughtful discussions and for sharing resources and experimental protocols. We thank the Johns Hopkins Sidney Kimmel Comprehensive Cancer Center Flow Cytometry and Cell Imaging Core Facilities supported by the Cancer Center Core Grant P30 CA006973. We also thank the Prostate Cancer Biorepository Network (PCBN), supported by the Department of Defense Prostate Cancer Research Program, DOD Award No W81XWH-10-2-0056 and W81XWH-10-2-0046. We acknowledge the use of tissues procured by the National Disease Research Interchange (NDRI) with support from NIH grant 2 U42 OD011158.

Financial Support

This work was supported by Department of Defense Prostate Cancer Research Program W81XWH-11-PCRP-IDA (PJH), The Patrick C. Walsh Prostate Cancer Fund (PJH), The Willowcroft Foundation (PJH), The Johns Hopkins Catalyst Award (PJH), The American Cancer Society 131356-RSG-17-160-01-CSM (PJH), The National Cancer Institute/National Institute of Health RO1CA211695-01A1 (PJH; BWS; TL; WNB; RMH), R01CA194024 (BHP), and R01CA201035 (DLJT), and the Commonwealth Foundation (BHP). WNB acknowledges support from the Prostate Cancer Foundation as the Clay and Lynn Hamlin Young Investigator. BHP acknowledges support from Susan G. Komen as a Komen Scholar.

References

1. Hanahan D, Weinberg RA. Hallmarks of cancer: the next generation. Cell. 2011;144:646–74. [PubMed: 21376230]
2. Kalluri R The biology and function of fibroblasts in cancer. Nature reviews Cancer. 2016;16:582–98. [PubMed: 27550820]
3. LeBleu VS, Kalluri R. A peek into cancer-associated fibroblasts: origins, functions and translational impact. Dis Model Mech. 2018;11.
4. Ridge SM, Sullivan FJ, Glynn SA. Mesenchymal stem cells: key players in cancer progression. Mol Cancer. 2017;16:31. [PubMed: 28148268]
5. Brennen WN, Zhang B, Kulac I, Kisteman LN, Antony L, Wang H, et al. Mesenchymal stem cell infiltration during neoplastic transformation of the human prostate. Oncotarget. 2017.
6. Pittenger MF, Mackay AM, Beck SC, Jaiswal RK, Douglas R, Mosca JD, et al. Multilineage potential of adult human mesenchymal stem cells. Science. 1999;284:143–7. [PubMed: 10102814]
7. Paunescu V, Bojin FM, Tatu CA, Gavriliuc OI, Rosca A, Gruia AT, et al. Tumour-associated fibroblasts and mesenchymal stem cells: more similarities than differences. J Cell Mol Med. 2011;15:635–46. [PubMed: 20184663]
8. Mishra PJ, Mishra PJ, Humeniuk R, Medina DJ, Alexe G, Mesirov JP, et al. Carcinoma-associated fibroblast-like differentiation of human mesenchymal stem cells. Cancer Res. 2008;68:4331–9. [PubMed: 18519693]
9. Kansy BA, Dissmann PA, Hemeda H, Bruderek K, Westerkamp AM, Jagalski V, et al. The bidirectional tumor--mesenchymal stromal cell interaction promotes the progression of head and neck cancer. Stem Cell Res Ther. 2014;5:95. [PubMed: 25115189]
10. Karnoub AE, Dash AB, Vo AP, Sullivan A, Brooks MW, Bell GW, et al. Mesenchymal stem cells within tumour stroma promote breast cancer metastasis. Nature. 2007;449:557–63. [PubMed: 17914389]
11. Prantl L, Muehlberg F, Navone NM, Song YH, Vykoukal J, Logothetis CJ, et al. Adipose tissue-derived stem cells promote prostate tumor growth. Prostate. 2010;70:1709–15. [PubMed: 20564322]
12. Suzuki K, Sun R, Origuchi M, Kanehira M, Takahata T, Itoh J, et al. Mesenchymal stromal cells promote tumor growth through the enhancement of neovascularization. Molecular medicine. 2011;17:579–87. [PubMed: 21424106]
13. Kucerova L, Matuskova M, Hlubinova K, Altanerova V, Altaner C. Tumor cell behaviour modulation by mesenchymal stromal cells. Mol Cancer. 2010;9:129. [PubMed: 20509882]
14. O'Connell JT, Sugimoto H, Cooke VG, MacDonald BA, Mehta AI, LeBleu VS, et al. VEGF-A and Tenascin-C produced by S100A4+ stromal cells are important for metastatic colonization. Proc Natl Acad Sci U S A. 2011;108:16002–7. [PubMed: 21911392]
15. Khakoo AY, Pati S, Anderson SA, Reid W, Elshal MF, Rovira II, et al. Human mesenchymal stem cells exert potent antitumorigenic effects in a model of Kaposi's sarcoma. J Exp Med. 2006;203:1235–47. [PubMed: 16636132]
16. Qiao L, Xu Z, Zhao T, Zhao Z, Shi M, Zhao RC, et al. Suppression of tumorigenesis by human mesenchymal stem cells in a hepatoma model. Cell Res. 2008;18:500–7. [PubMed: 18364678]
17. Ozdemir BC, Pentcheva-Hoang T, Carstens JL, Zheng X, Wu CC, Simpson TR, et al. Depletion of carcinoma-associated fibroblasts and fibrosis induces immunosuppression and accelerates pancreas cancer with reduced survival. Cancer cell. 2014;25:719–34. [PubMed: 24856586]

18. Schaeffer EM, Marchionni L, Huang Z, Simons B, Blackman A, Yu W, et al. Androgen-induced programs for prostate epithelial growth and invasion arise in embryogenesis and are reactivated in cancer. Oncogene. 2008;27:7180–91. [PubMed: 18794802]
19. Pritchard C, Mecham B, Dumpit R, Coleman I, Bhattacharjee M, Chen Q, et al. Conserved gene expression programs integrate mammalian prostate development and tumorigenesis. Cancer Res. 2009;69:1739–47. [PubMed: 19223557]
20. Orr B, Riddick AC, Stewart GD, Anderson RA, Franco OE, Hayward SW, et al. Identification of stromally expressed molecules in the prostate by tag-profiling of cancer-associated fibroblasts, normal fibroblasts and fetal prostate. Oncogene.31:1130–42.
21. Hurley PJ, Sundi D, Shinder B, Simons B, Hughes RM, Miller RM, et al. Germline Variants in Asporin Vary by Race, Modulate the Tumor Microenvironment and are Differentially Associated with Metastatic Prostate Cancer. Clin Cancer Res. 2015.
22. Rochette A, Boufaied N, Scarlata E, Hamel L, Brimo F, Whitaker HC, et al. Asporin is a stromally expressed marker associated with prostate cancer progression. Br J Cancer. 2017;116:775–84. [PubMed: 28152543]
23. Castellana B, Escuin D, Peiro G, Garcia-Valdecasas B, Vazquez T, Pons C, et al. ASPN and GJB2 Are Implicated in the Mechanisms of Invasion of Ductal Breast Carcinomas. J Cancer.3:175–83. [PubMed: 22514560]
24. Satoyoshi R, Kuriyama S, Aiba N, Yashiro M, Tanaka M. Asporin activates coordinated invasion of scirrhous gastric cancer and cancer-associated fibroblasts. Oncogene. 2014.
25. Wang L, Wu H, Wang L, Zhang H, Lu J, Liang Z, et al. Asporin promotes pancreatic cancer cell invasion and migration by regulating the epithelial-to-mesenchymal transition (EMT) through both autocrine and paracrine mechanisms. Cancer Lett. 2017;398:24–36. [PubMed: 28400334]
26. Kajikawa T, Yamada S, Tauchi T, Awata T, Yamaba S, Fujihara C, et al. Inhibitory effects of PLAP-1/asporin on periodontal ligament cells. Journal of dental research. 2014;93:400–5. [PubMed: 24453179]
27. Kizawa H, Kou I, Iida A, Sudo A, Miyamoto Y, Fukuda A, et al. An aspartic acid repeat polymorphism in asporin inhibits chondrogenesis and increases susceptibility to osteoarthritis. Nat Genet. 2005;37:138–44. [PubMed: 15640800]
28. Ding Q, Zhang M, Liu C. Asporin participates in gastric cancer cell growth and migration by influencing EGF receptor signaling. Oncology reports. 2015;33:1783–90. [PubMed: 25673058]
29. Simkova D, Kharaishvili G, Korinkova G, Ozdian T, Suchankova-Kleplova T, Soukup T, et al. The dual role of asporin in breast cancer progression. Oncotarget. 2016;7:52045–60. [PubMed: 27409832]
30. Hurley PJ, Marchionni L, Simons BW, Ross AE, Peskoe SB, Miller RM, et al. Secreted protein, acidic and rich in cysteine-like 1 (SPARCL1) is down regulated in aggressive prostate cancers and is prognostic for poor clinical outcome. Proc Natl Acad Sci U S A.109:14977–82.
31. Hurley PJ, Wilsker D, Bunz F. Human cancer cells require ATR for cell cycle progression following exposure to ionizing radiation. Oncogene. 2007;26:2535–42. [PubMed: 17043640]
32. Hurley PJ, Hughes RM, Simons B, Huang J, Miller RM, Shinder B, et al. Androgen Regulated SPARCL1 in the Tumor Microenvironment Inhibits Metastatic Progression. Cancer Res. 2015.
33. Guo C, Liu H, Zhang BH, Cadaneanu RM, Mayle AM, Garraway IP. Epcam, CD44, and CD49f distinguish sphere-forming human prostate basal cells from a subpopulation with predominant tubule initiation capability. PLoS One. 2012;7:e34219. [PubMed: 22514625]
34. Phinney DG. Isolation of mesenchymal stem cells from murine bone marrow by immunodepletion. Methods Mol Biol. 2008;449:171–86. [PubMed: 18370091]
35. Boregowda SV, Krishnappa V, Chambers JW, Lograsso PV, Lai WT, Ortiz LA, et al. Atmospheric oxygen inhibits growth and differentiation of marrow-derived mouse mesenchymal stem cells via a p53-dependent mechanism: implications for long-term culture expansion. Stem cells. 2012;30:975–87. [PubMed: 22367737]
36. Zhu H, Guo ZK, Jiang XX, Li H, Wang XY, Yao HY, et al. A protocol for isolation and culture of mesenchymal stem cells from mouse compact bone. Nat Protoc. 2010;5:550–60. [PubMed: 20203670]

37. Gundem G, Van Loo P, Kremeyer B, Alexandrov LB, Tubio JM, Papaemmanuil E, et al. The evolutionary history of lethal metastatic prostate cancer. Nature. 2015;520:353–7. [PubMed: 25830880]
38. Simons BW, Durham NM, Bruno TC, Grosso JF, Schaeffer AJ, Ross AE, et al. A human prostatic bacterial isolate alters the prostatic microenvironment and accelerates prostate cancer progression. J Pathol. 2015;235:478–89. [PubMed: 25348195]
39. Brennen WN, Kisteman LN, Isaacs JT. Rapid selection of mesenchymal stem and progenitor cells in primary prostate stromal cultures. Prostate. 2016;76:552–64. [PubMed: 26732992]
40. Karthaus WR, Iaquinta PJ, Drost J, Gracanin A, van Boxtel R, Wongvipat J, et al. Identification of multipotent luminal progenitor cells in human prostate organoid cultures. Cell. 2014;159:163–75. [PubMed: 25201529]
41. Chua CW, Shibata M, Lei M, Toivanen R, Barlow LJ, Bergren SK, et al. Single luminal epithelial progenitors can generate prostate organoids in culture. Nature cell biology. 2014;16:951–61, 1-4. [PubMed: 25241035]
42. Hughes RM, Simons BW, Hurley PJ. A Murine Orthotopic Allograft to Model Prostate Cancer Growth and Metastasis. Bio Protoc. 2017;7.
43. Johnson WE, Li C, Rabinovic A. Adjusting batch effects in microarray expression data using empirical Bayes methods. Biostatistics. 2007;8:118–27. [PubMed: 16632515]
44. Leek JT, Johnson WE, Parker HS, Jaffe AE, Storey JD. The sva package for removing batch effects and other unwanted variation in high-throughput experiments. Bioinformatics. 2012;28:882–3. [PubMed: 22257669]
45. Ritchie ME, Phipson B, Wu D, Hu Y, Law CW, Shi W, et al. limma powers differential expression analyses for RNA-sequencing and microarray studies. Nucleic acids research. 2015;43:e47. [PubMed: 25605792]
46. Tang T, Li L, Tang J, Li Y, Lin WY, Martin F, et al. A mouse knockout library for secreted and transmembrane proteins. Nat Biotechnol. 2010;28:749–55. [PubMed: 20562862]
47. Quante M, Tu SP, Tomita H, Gonda T, Wang SS, Takashi S, et al. Bone marrow-derived myofibroblasts contribute to the mesenchymal stem cell niche and promote tumor growth. Cancer cell. 2011;19:257–72. [PubMed: 21316604]
48. Kibel AS, Suarez BK, Belani J, Oh J, Webster R, Brophy-Ebbers M, et al. CDKN1A and CDKN1B polymorphisms and risk of advanced prostate carcinoma. Cancer research. 2003;63:2033–6. [PubMed: 12727815]
49. Tomoeda M, Yamada S, Shirai H, Ozawa Y, Yanagita M, Murakami S. PLAP-1/asporin inhibits activation of BMP receptor via its leucine-rich repeat motif. Biochem Biophys Res Commun. 2008;371:191–6. [PubMed: 18407830]
50. Awata T, Yamada S, Tsushima K, Sakashita H, Yamaba S, Kajikawa T, et al. PLAP-1/Asporin Positively Regulates FGF-2 Activity. Journal of dental research. 2015.
51. Luehders K, Sasai N, Davaapil H, Kurosawa-Yoshida M, Hiura H, Brah T, et al. The small leucine-rich repeat secreted protein Asporin induces eyes in Xenopus embryos through the IGF signalling pathway. Development. 2015;142:3351–61. [PubMed: 26443635]
52. Nakajima M, Kizawa H, Saitoh M, Kou I, Miyazono K, Ikegawa S. Mechanisms for asporin function and regulation in articular cartilage. J Biol Chem. 2007;282:32185–92. [PubMed: 17827158]
53. Yamada S, Tomoeda M, Ozawa Y, Yoneda S, Terashima Y, Ikezawa K, et al. PLAP-1/asporin, a novel negative regulator of periodontal ligament mineralization. J Biol Chem. 2007;282:23070–80. [PubMed: 17522060]
54. Grafe I, Alexander S, Peterson JR, Snider TN, Levi B, Lee B, et al. TGF-beta Family Signaling in Mesenchymal Differentiation. Cold Spring Harbor perspectives in biology. 2017.
55. Spaeth EL, Dembinski JL, Sasser AK, Watson K, Klopp A, Hall B, et al. Mesenchymal stem cell transition to tumor-associated fibroblasts contributes to fibrovascular network expansion and tumor progression. PLoS One. 2009;4:e4992. [PubMed: 19352430]
56. Zeisberg EM, Potenta S, Xie L, Zeisberg M, Kalluri R. Discovery of endothelial to mesenchymal transition as a source for carcinoma-associated fibroblasts. Cancer Res. 2007;67:10123–8. [PubMed: 17974953]

57. Barretina J, Caponigro G, Stransky N, Venkatesan K, Margolin AA, Kim S, et al. The Cancer Cell Line Encyclopedia enables predictive modelling of anticancer drug sensitivity. Nature. 2012;483:603–7. [PubMed: 22460905]

58. Cerami E, Gao J, Dogrusoz U, Gross BE, Sumer SO, Aksoy BA, et al. The cBio cancer genomics portal: an open platform for exploring multidimensional cancer genomics data. Cancer discovery. 2012;2:401–4. [PubMed: 22588877]

59. Gao J, Aksoy BA, Dogrusoz U, Dresdner G, Gross B, Sumer SO, et al. Integrative analysis of complex cancer genomics and clinical profiles using the cBioPortal. Sci Signal. 2013;6:pl1.

60. Ellis L, Ku S, Li Q, Azabdaftari G, Seliski J, Olson B, et al. Generation of a C57BL/6 MYC-Driven Mouse Model and Cell Line of Prostate Cancer. Prostate. 2016;76:1192–202. [PubMed: 27225803]

61. Kalamajski S, Aspberg A, Lindblom K, Heinegard D, Oldberg A. Asporin competes with decorin for collagen binding, binds calcium and promotes osteoblast collagen mineralization. Biochem J. 2009;423:53–9. [PubMed: 19589127]

62. Wu H, Jing X, Cheng X, He Y, Hu L, Wu H, et al. Asporin enhances colorectal cancer metastasis through activating the EGFR/src/cortactin signaling pathway. Oncotarget. 2016.

63. Maris P, Blomme A, Palacios AP, Costanza B, Bellahcene A, Bianchi E, et al. Asporin Is a Fibroblast-Derived TGF-beta1 Inhibitor and a Tumor Suppressor Associated with Good Prognosis in Breast Cancer. PLoS medicine. 2015;12:e1001871. [PubMed: 26327350]

Significance

Findings show that asporin regulates key properties of mesenchymal stromal cells including self-renewal and multipotency, and asporin expression by reactive stromal cells alters the tumor microenvironment and promotes metastatic progression.

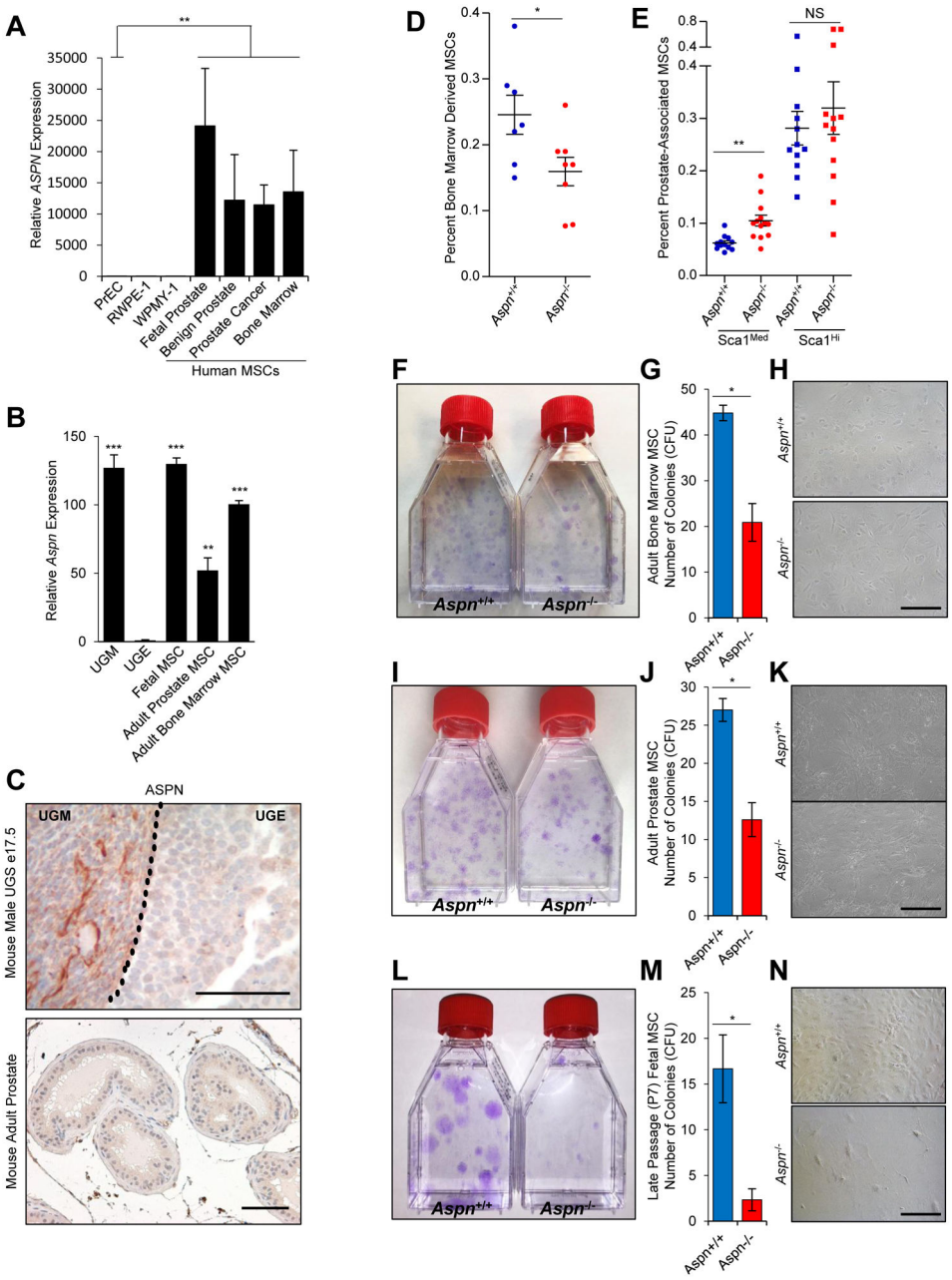

Figure 1.

ASPN is expressed in MSCs and regulates MSC self-renewal. A, Relative *ASPN* expression in human primary prostate epithelial cells (PrEC), a benign human prostate epithelial cell line (RWPE-1), a human prostate stromal cell line (WPMY-1), and primary human MSCs as measured by qRT-PCR. Statistical analyses performed using Welch's t-test (n≥3). B, Relative *Aspn* expression in mouse fetal prostate mesenchyme (UGM), mouse fetal prostate epithelium (UGE), and mouse MSCs as measured by qRT-PCR. Statistical analyses performed using one-way ANOVA with Tukey multiple comparison (n≥3). C, ASPN expression as measured by IHC in the urogenital sinus (UGS) and in adult mouse prostate. D, E, $Aspn^{+/+}$ and $Aspn^{-/-}$ (D) bone marrow and (E) prostates were analyzed by flow

cytometry for MSCs ($CD45^-$, $CD105^+$, $CD29^+$, and $Sca\text{-}1^+$). Statistical analyses performed using Student's t-test (n≥7). F-H, $Aspn^{+/+}$ and $Aspn^{-/-}$ adult bone marrow-derived MSCs were isolated and then plated at equal densities for CFU assays. Displayed are the average number of colonies formed per 2.5×10^3 cells plated. Statistical analyses performed using Student's t-test (n≥6). I-K, $Aspn^{+/+}$ and $Aspn^{-/-}$ adult prostate MSCs were isolated and then plated at equal densities for CFU assays. Statistical analyses performed using Student's t-test (n≥3). L-N, $Aspn^{+/+}$ and $Aspn^{-/-}$ fetal MSCs were isolated and then plated at equal densities for CFU assays. Statistical analyses performed using Student's t-test (n≥3). Graphs shown as mean±SEM, *P≤0.05, **P≤0.01, ***P≤0.001, NS=not significant, and black bars=100μM.

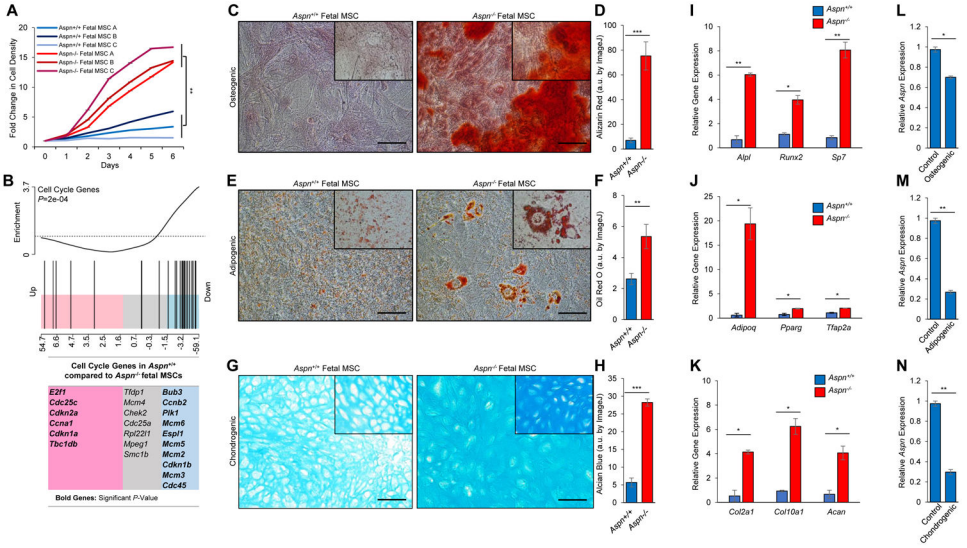

Figure 2.

ASPN restricts MSC proliferation and differentiation. A, Cell growth of *Aspn*$^{+/+}$ and *Aspn*$^{-/-}$ fetal MSCs. B, Gene set enrichment analysis (GSEA) of cell cycle genes in *Aspn*$^{+/+}$ and *Aspn*$^{-/-}$ fetal MSCs as determined from microarray data (n=3). C-H, *Aspn*$^{+/+}$ and *Aspn*$^{-/-}$ fetal MSCs were cultured in (C, D) osteogenic, (E, F) adipogenic, and (G, H) chondrogenic differentiation-inducing media and then stained for Alizarin Red, Oil Red O, and Alcian Blue, respectively. Staining was quantified using ImageJ (n=3). I-K, Expression of (I) osteogenic, (J) adipogenic, and (K) chondrogenic differentiation-induced genes in *Aspn*$^{+/+}$ and *Aspn*$^{-/-}$ fetal MSCs as determined by qRT-PCR (n≥3). L-N, *Aspn* expression in *Aspn*$^{+/+}$ fetal MSCs cultured in (L) osteogenic, (M) adipogenic, and (N) chondrogenic differentiation-inducing media (n=3). Statistical analyses in A and C-N performed using Student's t-test (mean±SEM; **P*≤0.05, ***P*≤0.01, ****P*≤0.001; n≥3). Black bars=100μM.

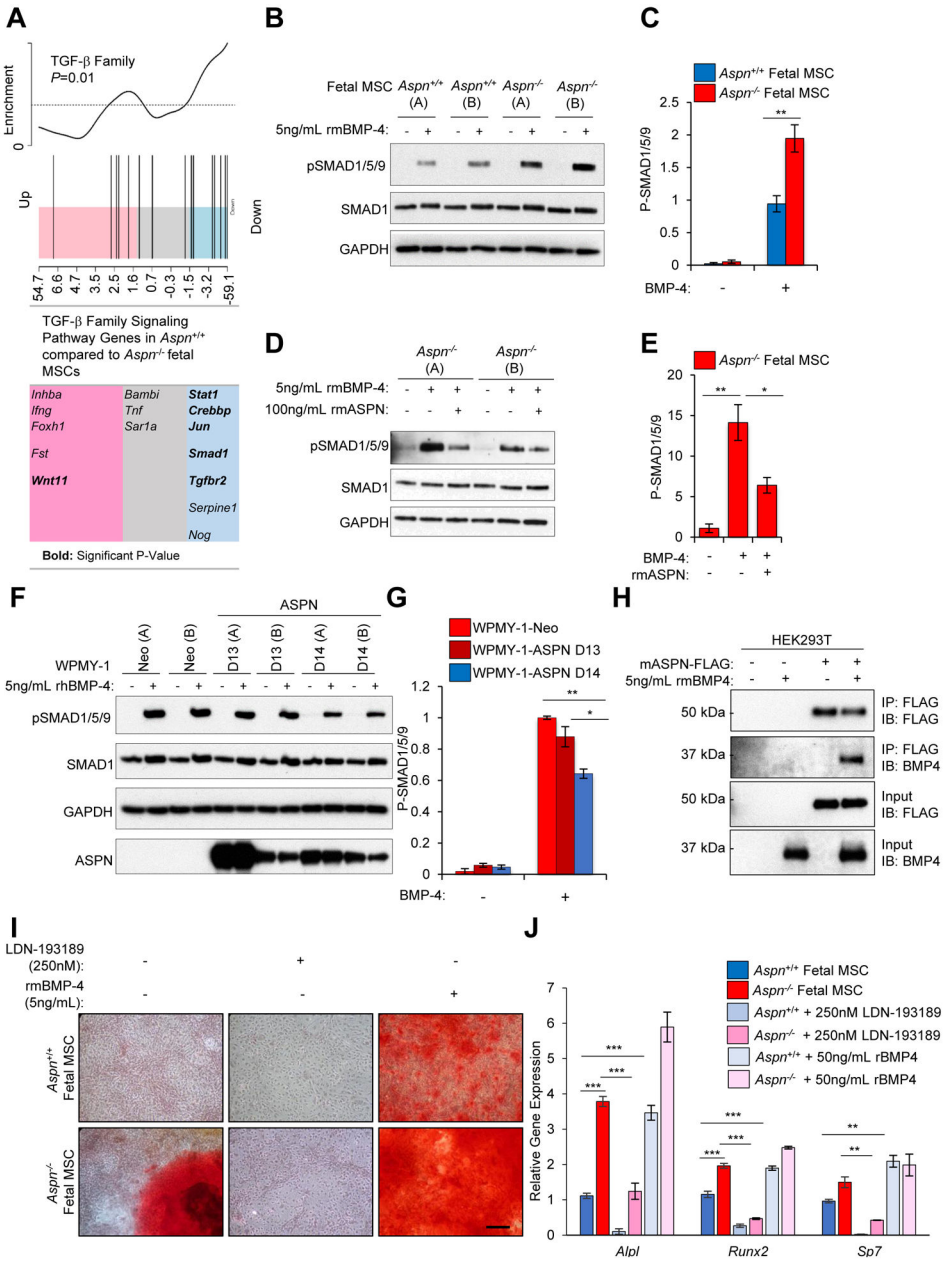

Figure 3.

ASPN binds to BMP-4 and restricts BMP-4-induced signaling. A, GSEA of TGF-β family pathway genes in *Aspn*$^{+/+}$ and *Aspn*$^{-/-}$ fetal MSCs as determined from microarray (n=3). B, C, BMP-4-induced signaling in *Aspn*$^{+/+}$ and *Aspn*$^{-/-}$ fetal MSCs (A and B represent independently derived MSCs) as measured by immunoblotting and quantified using ImageJ. *Aspn*$^{+/+}$ and *Aspn*$^{-/-}$ fetal MSCs were serum-depleted and then incubated with recombinant mouse BMP-4 (5ng/mL) for 30 minutes. Statistical analyses performed using Student's t-test (n≥3). D, E, Recombinant mouse ASPN restricts BMP-4-induced signaling in *Aspn*$^{-/-}$ fetal MSCs as measured by immunoblotting and quantified using ImageJ. *Aspn*$^{+/+}$ and *Aspn*$^{-/-}$ fetal MSCs were serum-depleted and then incubated with recombinant mouse BMP-4

(5ng/mL) with vehicle or recombinant mouse ASPN (100ng/mL) for 30 minutes. Statistical analyses performed using Student's t-test (n≥2). F, G, BMP-4-induced signaling in WPMY-1-Neo, WPMY-1-ASPN D13, and WPMY-1ASPN D14 (A and B represent independently derived clones) as measured by immunoblotting and quantified using ImageJ. WPMY-1-Neo, WPMY-1-ASPN D13, and WPMY-1ASPN D14 were serum-depleted and then incubated with recombinant human BMP-4 (5ng/mL) for 30 minutes. Statistical analyses performed using one-way ANOVA with Tukey multiple comparison (n≥3). H, Co-immunoprecipitation of ASPN and BMP-4. FLAG tagged mouse ASPN was transfected in HEK293T cells and then incubated with recombinant mouse BMP-4. ASPN was immunoprecipitated with anti-FLAG beads and then examined by immunoblotting for ASPN and BMP-4 (n=2). I, $Aspn^{+/+}$ and $Aspn^{-/-}$ fetal MSCs were cultured in osteogenic-inducing media with either vehicle, 250nM LDN-193189, or recombinant mouse BMP4 (5ng/mL) and then stained for Alizarin Red. J, $Aspn^{+/+}$ and $Aspn^{-/-}$ fetal MSCs were cultured in osteogenic-inducing media with either vehicle, 250nM LDN-193189, or recombinant mouse BMP4 (5ng/mL) and then examined for osteogenic-induced genes by qRT-PCR. Statistical analyses performed using one-way ANOVA with Tukey multiple comparison (n≥3). Graphs shown as mean±SEM, $*P \leq 0.05$, $**P \leq 0.01$, $***P \leq 0.001$, and black bars=100μM.

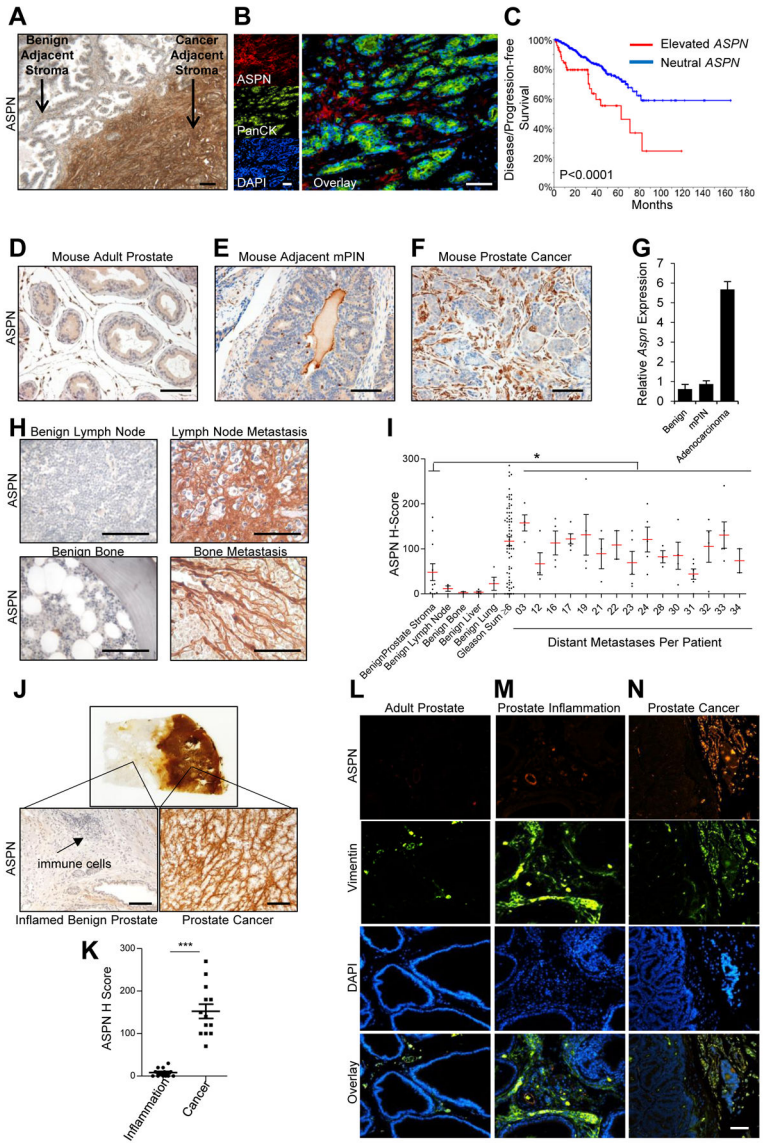

Figure 4.

ASPN is expressed in primary and metastatic prostate cancer tumor microenvironments, but not in the microenvironment of prostate inflammation. A, ASPN expression in human prostate cancer as measured by IHC. B, ASPN (red), pancytokeratin (green), and DAPI (blue) expression in human prostate cancer as measured by immunofluorescence (IF). C, Elevated *ASPN* (amplification, gain, expression>2) was associated with worse disease/progression-free survival in TCGA data as determined by Kaplan-Meier survival curves and visualized on cBioPortal (n=491; Logrank Test). D-F, ASPN expression in (D) mouse adult prostate, (E) murine prostatic intraepithelial neoplasia (mPIN) in the TRAMP model, and (F) mouse prostate adenocarcinoma in the TRAMP model as measured by IHC and (G) qRT-PCR. H, I, Mean ASPN H-score in prostate cancer metastases from the PELICAN rapid autopsy study of prostate cancer (n=15 patients with an average of 4 metastases per patient), benign adjacent prostate stroma (n=11), benign bone (n=2), benign lymph node (n=3), benign lung (n=4), and benign liver (n=4) as measured by IHC. Historical controls of stroma

adjacent to benign prostate and stroma adjacent to Gleason grade ≥6 prostate cancer (G≥6) were measured and calculated using the same methodology and included for comparison. Statistical analyses performed using one-way ANOVA with Newman-Keuls multiple comparison. J, ASPN expression in human prostate inflammation and human prostate cancer as measured by IHC on radical prostatectomy sections that contained regions of both chronic inflammation and prostate cancer in non-overlapping locations. K, Quantification of ASPN expression by IHC (H-score) in stroma adjacent to inflammation and stroma adjacent to cancer on single sections from radical prostatectomy sections. Statistical analyses performed using Student's t-test (n=13 patients). L-N, ASPN (red), Vimentin (green), and DAPI (blue) expression in mouse adult prostate (L), CP1 *E. coli*-induced mouse prostate inflammation (M), and mouse prostate adenocarcinoma in the TRAMP model (N) as measured by IF. Graphs shown as mean±SEM, **P*≤0.05, ***P*≤0.01, ****P*≤0.001, and black and white bars=100μM.

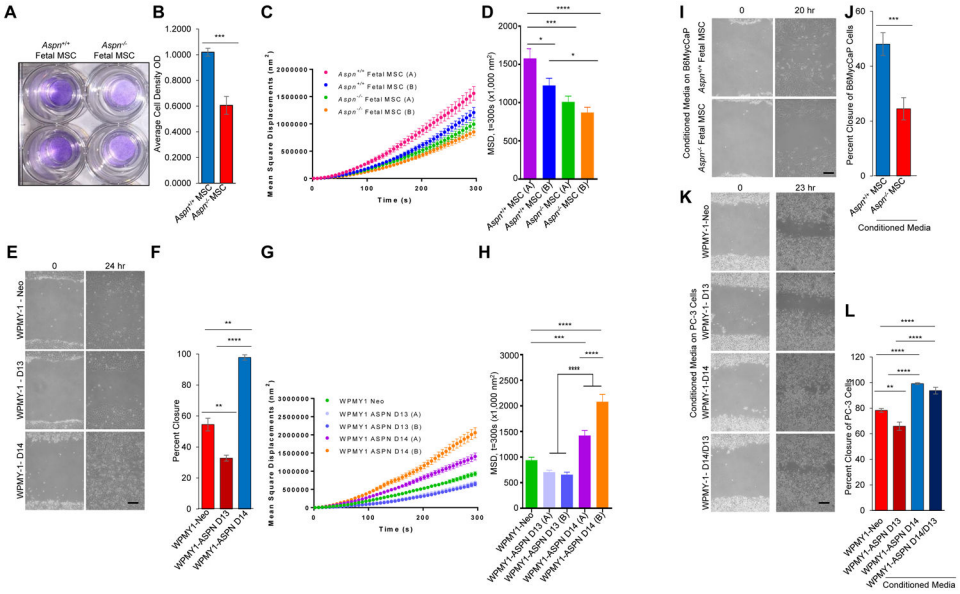

Figure 5.

ASPN enhances MSC and cancer cell migration. A, B, Migration of *Aspn*$^{+/+}$ and *Aspn*$^{-/-}$ fetal MSCs across a membrane. Statistical analyses performed using Student's t-test (n=3). C, D, Cytoskeletal remodeling as measured by (C) mean square displacement and (D) analyzed at t=300s nm^2 in *Aspn*$^{+/+}$ and *Aspn*$^{-/-}$ fetal MSCs. Statistical analyses performed using one-way ANOVA with Tukey multiple comparison (n≥3). E, F, Migration of WPMY-1-Neo, WPMY-1-ASPN D13, and WPMY-1-ASPN D14 as determined by scratch assay. Statistical analyses performed using one-way ANOVA with Tukey multiple comparison (n≥9). G, H, Cytoskeletal remodeling as measured by (G) mean square displacement and (H) analyzed at t=300 nm^2 in WPMY-1-Neo, WPMY-1-ASPN D13, and WPMY-1-ASPN D14 (n=2 independent clones per experimental group). Statistical analyses performed using one-way ANOVA with Tukey multiple comparison (n≥3). I, J, Migration of B6MycCaP cells in conditioned media from *Aspn*$^{+/+}$ and *Aspn*$^{-/-}$ fetal MSCs as determined by scratch assay. Statistical analyses performed using Student's t-test (n=3). K, L, Migration of PC-3 cells in conditioned media from WPMY-1-Neo, WPMY-1-ASPN D13, WPMY-1-ASPN D14, and a 1:1 mix from WPMY-1-ASPN D13:WPMY-1-ASPN D14 cells. Statistical analyses performed using one-way ANOVA with Tukey multiple comparison (n≥9). Graphs shown as mean±SEM, **P*≤0.05, ***P*≤0.01, ****P*≤0.001, and black bars=100μM.

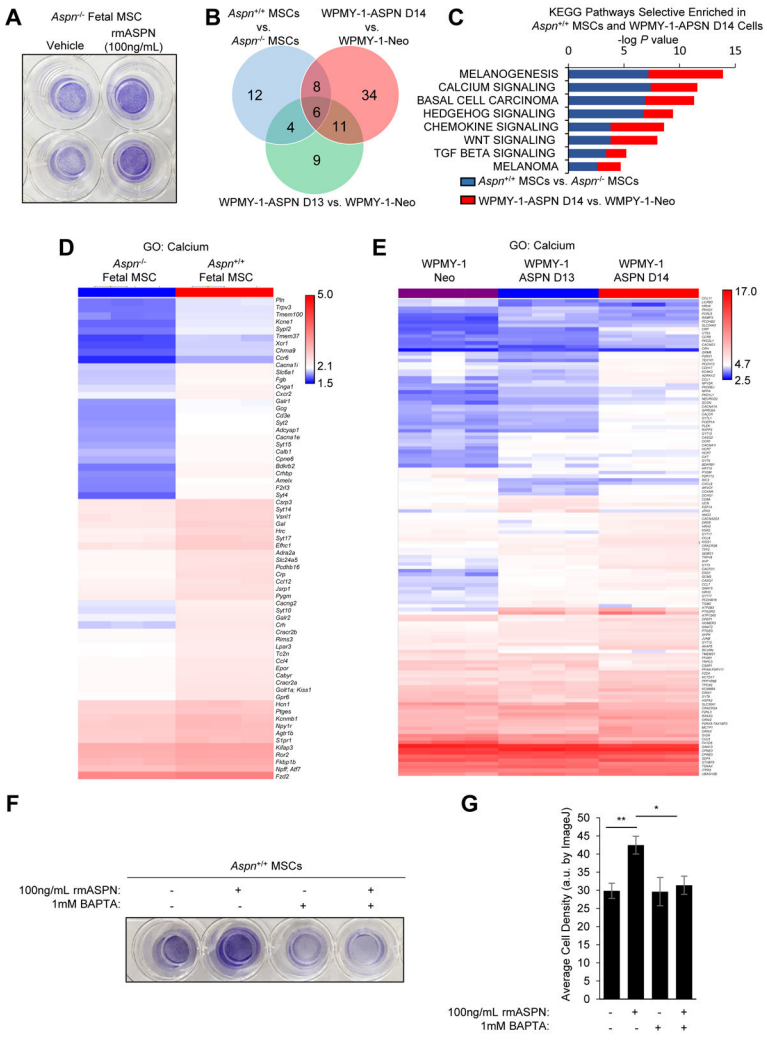

Figure 6.

ASPN-mediated migration is calcium-dependent. A, Migration of *Aspn*$^{-/-}$ cells in low calcium media with vehicle or 100ng/mL recombinant mouse ASPN as determined by transwell assay. B, Venn Diagram of altered KEGG Pathways between differentially expressed genes in *Aspn*$^{+/+}$ MSCs compared to *Aspn*$^{-/-}$ MSCs as well as in WPMY-1-ASPN D14 compared to WPMY-1-ASPN Neo and in WPMY-1-ASPN D13 compared to WPMY-1-ASPN Neo. C, KEGG Pathway enrichment selective to *Aspn*$^{+/+}$ MSCs and WPMY-1-ASPN D14 cells compared to cells deficient for ASPN. D, Hierarchical clustering of GO calcium-related genes in *Aspn*$^{+/+}$ and *Aspn*$^{-/-}$ fetal MSCs. E, Hierarchical clustering of GO calcium-related genes in WPMY-1-ASPN D14, WPMY-1-ASPN Neo, and WPMY-1-ASPN D13 cells. F,G, Migration of *Aspn*$^{-/-}$ cells in low calcium media with vehicle, 100ng/mL recombinant mouse ASPN, 1mM BAPTA, or ASPN and BAPTA as determined by transwell assay. Quantification by ImageJ. Statistical analyses performed using one-way ANOVA with Newman-Keuls multiple comparison (mean±SEM; * $P \leq 0.05$, ** $P \leq 0.01$; n≥3).

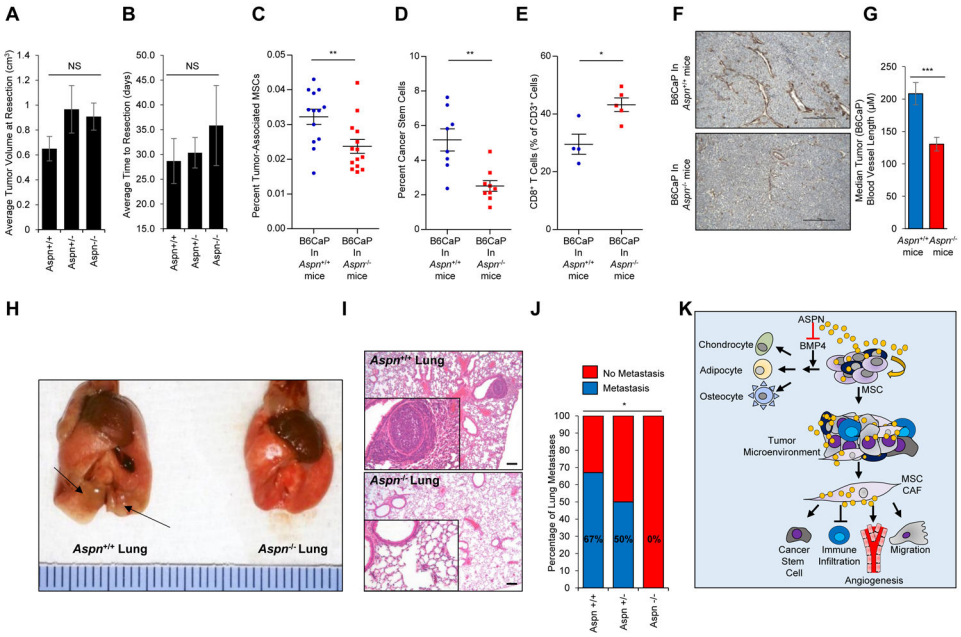

Figure 7.

ASPN regulates the tumor microenvironment and promotes metastatic development. A, B, Tumor volume (A) and time to resection (B) of B6CaP subcutaneous allografts in *Aspn*$^{+/+}$ (n=6), *Aspn*$^{+/-}$ (n=6), and *Aspn*$^{-/-}$ (n=6) mice. Statistical analyses performed using one-way ANOVA with Tukey multiple comparison. C, Percent tumor-associated MSCs (CD45^{-}, CD105^{+}, CD29^{+}, and Sca-1^{+}) in B6CaP subcutaneous allografts from *Aspn*$^{+/+}$ and *Aspn*$^{-/-}$ mice as measured by flow cytometry. Statistical analyses performed using Student's t-test (n≥13). D, Percent cancer stem cells (CD45^{-}, CD105^{-}, CD31^{-}, CD29^{+}, Sca-1^{+}, CD44^{+}) in B6CaP subcutaneous allografts from *Aspn*$^{+/+}$ and *Aspn*$^{-/-}$ mice as measured by flow cytometry. Statistical analyses performed using Student's t-test (n≥8). E, CD8^{+} T cells as a percent of CD3^{+} cells in B6CaP subcutaneous allografts from *Aspn*$^{+/+}$ and *Aspn*$^{-/-}$ mice as measured by flow cytometry. Statistical analyses performed using Student's t-test (n≥4). F, SMAα positive vasculature detected by IHC of B6CaP subcutaneous allografts from *Aspn*$^{+/+}$ and *Aspn*$^{-/-}$ mice. G, Quantification of vasculature length in B6CaP subcutaneous allografts from *Aspn*$^{+/+}$ and *Aspn*$^{-/-}$ mice. Statistical analyses performed using Student's t-test (n≥4). H, I, Photograph (H) and H&E (I) of lungs from *Aspn*$^{+/+}$ and *Aspn*$^{-/-}$ mice with B6CaP allograft. J, Percentage of *Aspn*$^{+/+}$ (4/6), *Aspn*$^{+/-}$ (3/6), and *Aspn*$^{-/-}$ (0/6) mice with lung metastases from B6CaP subcutaneous allografts as determined by H&E. Statistical analyses performed using Chi-squared test. K, Schematic of the role of ASPN in MSCs and metastasis. Graphs shown as mean±SEM, **P*≤0.05, ***P*≤0.01, ****P*≤0.001, NS=not significant, and black bars=100μM.

Key Resources

REAGENT or RESOURCE	SOURCE	IDENTIFIER
Antibodies		
Rabbit Anti-ASPN antibody	Sigma Prestige	Cat# HPA008435 RRID:AB_1845112
Mouse Anti-Vimentin antibody	Sigma	Cat# V2258 RRID:AB_261856
Rabbit anti-phospho SMAD1/5/9 antibody	Cell Signaling Technology	Cat# 13820 RRID:AB_2493181
Rabbit anti-SMAD1 antibody	Cell Signaling Technology	Cat# 9743 RRID:AB_2107780
Mouse anti-GAPDH antibody	Santa Cruz Biotechnology	Cat# sc-32233 RRID:AB_627679
Mouse anti-CK8 antibody	Covance Research Products Inc	Cat# MMS-162P-250 RRID:AB_291334
Rabbit anti-CK14 antibody	Covance Research Products Inc	Cat# PRB-155P RRID:AB_292096
Rabbit anti-Ki67 antibody	Abcam	Cat# ab15580 RRID:AB_443209
Mouse anti-FLAG	Sigma	Cat# F1804
Rabbit anti-BMP4	R&D	Cat# MAB5020
Mouse anti-SMA	Dako	Cat# M085129
APC/Cy7 Rat anti-mouse CD45 antibody	BioLegend	Cat# 103115 RRID:AB_312980
APC Rat anti-mouse CD105 antibody	BioLegend	Cat# 120413 RRID:AB_2277915
PE/Cy7 Armenian Hamster anti-mouse/rat CD29 antibody	BioLegend	Cat# 102221 RRID:AB_528789
FITC Rat anti-mouse Ly-6A/E (Sca-1) antibody	BioLegend	Cat# 108105 RRID:AB_313342
Ly6G	BioLegend	Clone 1A8
Ly6C	BioLegend	Clone HK1.4
CD11b	BioLegend	Clone M1/70
CD11c	BioLegend	Clone N418
CCR2	BioLegend	Clone SA203G11
F4/80	BioLegend	Clone BM8
CD3	BD Pharmingen	Clone 145-2C11
CD4	BioLegend	Clone GK1.5
CD8a	BioLegend	Clone 53-6.7
FoxP3	BioLegend	Clone 150D
CD44	BioLegend	Clone IM7
ImmPRESS HRP anti-mouse IgG antibody, made in Horse	Vector Laboratories	Cat# MP-7402 RRID:AB_2336528
ImmPRESS HRP anti-rabbit IgG antibody, made in Horse	Vector Laboratories	Cat# MP-7401 RRID:AB_2336529
F(ab)2-Goat anti-Mouse IgG (H+L) Cross-Adsorbed Secondary Antibody, Alexa Fluor 488	Thermo Fisher Scientific	Cat# A-11017 RRID:AB_2534084
Donkey anti-Rabbit IgG (H+L) Highly Cross-Adsorbed Secondary Antibody, Alexa Fluor 594	Thermo Fisher Scientific	Cat# A-21207 RRID:AB_141637
IgG agarose	Sigma	Cat# A0919
anti-FLAG M2 magnetic beads	Sigma	Cat# M8823
3x FLAG peptide	Sigma	Cat# F4799
Bacterial and Virus Strains		
CP1 *E. coli* strain	Brian W. Simons (Simons et al., 2015)	
Biological Samples		

REAGENT or RESOURCE	SOURCE	IDENTIFIER
Human Primary Prostate Cancer	Mayo Clinic Progression cohort (Hurley et al., 2016)	
Metastatic Prostate Cancer TMA	PELICAN rapid autopsy study of prostate cancer	
Matched prostate inflammation & cancer tissue	Johns Hopkins School of Medicine	
Chemicals, Peptides, and Recombinant Proteins		
RGD-coated microbeads	Steven S. An (An et al., 2004)	
FuGENE HD Transfection Reagent	Promega	Cat# E2311
LIVE/DEAD Fixable Aqua Dead Cell Stain kit (405nm excitation)	Thermo Fisher Scientific	Cat# L34957
MesenCult Osteogenic Stimulatory Kit (Mouse)	STEMCELL Technologies	Cat# 05504
MesenCult Adipogenic Stimulatory Supplement (Mouse)	STEMCELL Technologies	Cat# 05503
MesenCult ACF Chondrogenic Differentiation Medium	STEMCELL Technologies	Cat# 05455
Alizarin Red Staining solution	Millipore	Cat# TMS-008-C
Oil Red O solution	Sigma	Cat# O1391
Alcian-Blue Staining solution	Millipore	Cat# TMS-010-C
Recombinant Human BMP4	Peprotech	Cat# 120-05
Recombinant Mouse BPM4	R & D	Cat#5020-BP
Recombinant Mouse ASPN generated in 293T cells	Origene	Custom
Matrigel, Growth Factor Reduced (GFR)	Corning	Cat# 356230
Recombinant Mouse EGF	BioLegend	Cat# 713108
Y-27632 (ROCK inhibitor)	STEMCELL Technologies	Cat# 72302
5α-Androstan-17β-ol-3-one (DHT)	Sigma	Cat# A8380
A83-01 (TGFb inhibitor)	Tocris	Cat# 2939
Advanced DMEM/F12	Thermo Fisher Scientific	Cat# 12634-010
50X B-27 Supplement	Life Technologies	Cat# 17504-044
GlutaMAX	Life Technologies	Cat# 35050-079
HEPES	Life Technologies	Cat# 15630-080
Penicillin/Streptomycin (10,000 U/mL)	Life Technologies	Cat# 15140-122
10X Collagenase/Hyaluronidase	STEMCELL Technologies	Cat# 07912
Dispase (5 U/mL)	STEMCELL Technologies	Cat# 07913
10X DNAse I	STEMCELL Technologies	Cat# 07900
Thiazolyl Blue Tetrazolium Bromide	Sigma	Cat# M2128
Target Retrieval Solution, Ready to Use	Dako	Cat# S1700
Protein Block Serum-Free	Dako	Cat# X0909
Antibody Diluent Reagent Solution, Ready-to-use	Invitrogen	Cat# 003218
ImmPACT DAB (3,3'-Diaminobenzidine) Peroxidase Substrate	Vector Laboratories	Cat# SK-4105
VECTASHIELD HardSet Antifade Mounting Medium with DAPI counterstain	Vector Laboratories	Cat# H-1500
FcR Blocking Reagent, mouse	Miltenyi	Cat# 130-092-575
TaqMan Fast Advanced Master Mix	Thermo Fisher Scientific	Cat# 4444557
SimplyBlue SafeStain	Invitrogen	Cat# LC6060
Critical Commercial Assays		
Pierce BCA Protein Assay Kit, Reducing Agent Compatible	Thermo Fisher Scientific	Cat# 23250

REAGENT or RESOURCE	SOURCE	IDENTIFIER
SuperSignal West Pico PLUS Chemiluminescent Substrate	Thermo Fisher Scientific	Cat# 34580
QCM 24-well Colorimetric Cell Migration Assay	Millipore	Cat# ECM508
RNeasy Plus Mini Kit	Qiagen	Cat# 74134
Ready-To-Go You-Prime-First-Strand Beads	GE Healthcare	Cat# 27-9264-01
Amicon Ultra-4 10K Centrifugal Filter Device	Millipore	Cat# UFC801008
EasySep Mouse Mesenchymal Stem/Progenitor Cell Enrichment Kit	STEMCELL Technologies	Cat# 19771
MesenCult Expansion Kit (Mouse)	STEMCELL Technologies	Cat# 05513
Deposited Data		
SuperSeries (GSE109646)	This study	GEO database
Experimental Models: Cell Lines		
Human: WPMY-1	ATCC	
Human: WPMY-1-ASPN variants	Paula J. Hurley (Hurley et al., 2016)	
Human: MSCs (various sources)	W. Nathaniel Brennen (Brennen et al., 2017)	
Human: PC-3	ATCC	
Human: DU-145	ATCC	
Mouse: MSCs (various sources)	this study	
Mouse: B6MycCaP	Leigh Ellis (Ellis et al., 2016)	
Mouse: TRAMP-C2	ATCC	
Mouse: B6CaP organoids	this study	
Experimental Models: Organisms/Strains		
C57BL/6J mice	Jackson Labs	
B6;129S5-*Aspn* ^{tm1Lex}/Mmucd mice	Mutant Mouse Regional Resource Center (UC Davis)	
C57BL/6-Tg(TRAMP)8247Ng/J mice	Jackson Labs	
Oligonucleotides		
murine *Aspn* wild-type specific forward primer	5’ AGTCTACTTTGCCACATTCAC C 3’	
murine *Aspn* wild-type specific reverse primer	5’ GCTTTTGGCTGTGTGCTCTGC 3’	
murine *Aspn* mutation specific forward primer	5’CGAGAGTAACATTGGCACCC AAATG 3	
murine *Aspn* mutation specific reverse primer	5’ GCAGCGCATCGCCTTCTATC 3’	
Random hexamer primers	Promega	Cat# C118A
Human ASPN TaqMan qRT-PCR Gene Expression assay	Thermo Fisher Scientific	ID# Hs01550903_m1
Human HPRT1 TaqMan qRT-PCR Gene Expression assay	Thermo Fisher Scientific	ID# Hs02800695_m1
Human GAPDH TaqMan qRT-PCR Gene Expression assay	Thermo Fisher Scientific	ID# Hs02758991_g1
Mouse Aspn TaqMan qRT-PCR Gene Expression assay	Thermo Fisher Scientific	ID# Mm00445939_m1
Mouse Alpl TaqMan qRT-PCR Gene Expression assay	Thermo Fisher Scientific	ID# Mm00475834_m1
Mouse Runx2 TaqMan qRT-PCR Gene Expression assay	Thermo Fisher Scientific	ID# Mm00501584_m1
Mouse Sp7 TaqMan qRT-PCR Gene Expression assay	Thermo Fisher Scientific	ID# Mm04209856_m1

REAGENT or RESOURCE	SOURCE	IDENTIFIER
Mouse Adipoq TaqMan qRT-PCR Gene Expression assay	Thermo Fisher Scientific	ID# Mm00456425_m1
Mouse Pparg TaqMan qRT-PCR Gene Expression assay	Thermo Fisher Scientific	ID# Mm00440940_m1
Mouse Tfap2a TaqMan qRT-PCR Gene Expression assay	Thermo Fisher Scientific	ID# Mm00495574_m1
Mouse Col2a1 TaqMan qRT-PCR Gene Expression assay	Thermo Fisher Scientific	ID# Mm01309565_m1
Mouse Col10a1 TaqMan qRT-PCR Gene Expression assay	Thermo Fisher Scientific	ID# Mm00487041_m1
Mouse Acan TaqMan qRT-PCR Gene Expression assay	Thermo Fisher Scientific	ID# Mm00545794_m1
Mouse Dcn TaqMan qRT-PCR Gene Expression assay	Thermo Fisher Scientific	ID# Mm00514535_m1
mouse Bgn TaqMan qRT-PCR Gene Expression assay	Thermo Fisher Scientific	ID# Mm01191753_m1
mouse Ecm2 TaqMan qRT-PCR Gene Expression assay	Thermo Fisher Scientific	ID# Mm01349471_m1
mouse Hprt1 TaqMan qRT-PCR Gene Expression assay	Thermo Fisher Scientific	ID# Mm03024075_m1
mouse Gapdh TaqMan qRT-PCR Gene Expression assay	Thermo Fisher Scientific	ID# Mm99999915_g1
Recombinant DNA		
pIRESneo3 vector	Clontech	Cat# 631621
ASPN (NM_017680) Human cDNA clone	OriGene	Cat# SC321136
Software and Algorithms		
ImageJ	NIH	https://fiji.sc
PRISM	Graphpad	https://ww.graphpad.com
RStudio	RStudio Team	http://www.rstudio.com
FlowJo	FLOWJO LLC	FlowJo
NIS Elements (vAR 3.0)	Nikon	https://www.nikoninstruments.com
StepOne Software (v2.3)	Applied Biosystems (Thermo Fisher Scientific)	https://www.thermofisher.com
Transcriptome Analysis Console (TAC, v4.0)	Thermo Fisher Scientific	https://www.thermofisher.com